TÜBİTAK

Turkish Journal of Earth Sciences

http://journals.tubitak.gov.tr/earth/

Research Article

Turkish J Earth Sci
(2024) 33:
© TÜBİTAK
doi:/yer-2308-16

Derivation of a 1-D seismic velocity model for the Lake Van region

Mehveş Feyza AKKOYUNLU[1,*], Bülent KAYPAK[2], Bülent ORUÇ[3], Doğan KALAFAT[4]

[1]Kandilli Observatory and Earthquake Research Institute, Regional Earthquake-Tsunami Monitoring Centre (RETMC), İstanbul, Turkiye

[2]Department of Geophysical Engineering, Faculty of Engineering, Ankara University, Ankara, Turkiye

[3]Department of Geophysical Engineering, Faculty of Engineering, Kocaeli University, Kocaeli, Turkiye

[4]Kandilli Observatory and Earthquake Research Institute, Regional Earthquake-Tsunami Monitoring Centre (RETMC), İstanbul, Turkiye

Received: 30.08.2023 • **Accepted/Published Online:** 16.01.2024 • **Final Version:** 00.00.2024

Abstract: We present a detailed one-dimensional (1-D) velocity model of the Lake Van Basin and its surrounding region, alongside precise hypocenter locations, utilizing seismic data from the aftershocks of the 23 October 2011 Lake Van earthquake (Mw = 7.1). The 1-D minimum velocity model is computed by the VELEST program by analyzing body wave traveltimes and station corrections. Encompassing a geographical area of 180 × 90 km² centered around Lake Van, the study incorporated seismic data from 10 newly deployed stations, complementing the existing network of the Kandilli Earthquake Research Institute. A comprehensive manual analysis was conducted on a dataset comprising 7643 events occurring between 23 October 2011 and 21 January 2015. Among these, 1193 well-located events recorded by 16 stations were selected, encompassing 48,387 P-wave and 26,913 S-wave arrival times. The iterative simultaneous inversion technique was applied to refine velocity and hypocenter parameters while mitigating the influence of near-surface velocity heterogeneity and station elevation through station corrections. The resulting 1-D velocity model delineates eight distinct layers up to a depth of 39 km, including a 3-km-thick sedimentary layer, while determining the V_P/V_S ratio for each layer. Rigorous testing procedures were implemented to ensure the stability and accuracy of the velocity structure and aftershock locations. The relocation of the aftershock sequence using the new 1-D velocity model revealed significant shifts in the distribution pattern, notably concentrating relocated events towards the vicinity of the main shock area. This study underscores the efficacy of the VELEST software in deriving a robust 1-D velocity model and refining hypocenter locations for the Lake Van region. The insights gained enhance our understanding of the region's seismotectonic and have implications for seismic hazard assessment and risk mitigation strategies.

Key words: Van earthquake, crustal model, relocation, 1-D velocity model, V_P/V_S ratio, Lake Van

1. Introduction

Well-constrained hypocentral parameters (latitude, longitude, depth, and origin time) are essential for most seismological and earthquake hazard studies. Velocity model errors affect Local earthquake locations more due to seismic arrivals passage through the heterogeneous crust and uppermantle.

The 1-D seismic velocity models are necessary for accurate earthquake locations at many real-time seismological centers. Reliable earthquake locations are essential to analyze seismicity and characterize active faults to understand the tectonic regime of a region. Most earthquake catalogs provided by seismic networks are based on layered 1-D velocity models. Scattering in the earthquake locations may be caused by errors in station parameters (location and timing errors), misidentification of seismic phases, and velocity models in earthquake location computation (Husen and Hardebeck, 2010).

Additionally, 1-D seismic velocity models are essential as initial reference models for 3-D local earthquake tomography studies. A high-quality data set, well-identified seismic phases, and an accurate velocity model are crucial for reliable earthquake locations. Using high-quality arrival times from well-constrained earthquake locations to derive seismic velocity models has led to a minimum 1-D model (Kissling, 1988).

A minimum 1-D model can be obtained from simultaneous inversion for earthquake location, seismic velocities, and station delays by solving the coupled hypocenter-velocity problem. To derive a reliable 1-D model, an extensive range of 1-D velocity models are tested (Kissling et al., 1994). The minimum 1-D model

* Correspondence: Feyza.Akkoyunlu@bogazici.edu.tr

represents average seismic velocities for each layer sampled by ray distribution. Station delays compensate for near-surface velocity changes under stations and large-scale systematic variations of seismic velocities (Husen et al., 1999). While 1-D velocity models offer the advantages of computational simplicity and straightforward interpretation, they are constrained by their inability to account for lateral variations in velocity, representing a significant limitation in their application. While numerous studies have examined the crust and uppermost mantle structure in Eastern Anatolia using various methods at a broader scale, most of these investigations have predominantly focused on the western segment of the Lake Van region. The initial 1-D crustal velocity model of Turkelli et al. (2003) was obtained from a grid search technique using the ETSE array data covering the area west of Lake Van. Zor et al. (2003) investigated the crustal structure of the Eastern Anatolian Plateau using receiver functions. They found that the average crustal thickness is 45 km, and the average crustal shear velocity is 3.7 km/s for the Eastern Anatolian Plateau. Al Lazki et al. (2004) performed the uppermantle P-wave (Pn) velocities method and observed large-scale (approximately 500 km) low Pn velocity structures (<8.0 km/s). Crustal and uppermantle seismic discontinuities beneath Eastern Türkiye were imaged using the S-wave receiver function by Angus et al. (2006). They interpreted that Moho depth ranges from between 30 and 55 km. The 1-D crustal model derived by Pınar et al. (2007) was an average crust model based on previous studies. Anomalously high V_P/V_S ratios have previously been reported in Eastern Anatolia and attributed to volcanic activity in the region and partial melt in the crust at a depth of 40 km (Salah et al., 2011). To investigate earthquake clustering and time-dependent seismicity patterns in the region, Toker and Ecevitoğlu (2012) utilized data from 6500 aftershocks recorded at the VANB-Broadband station of Kandilli Observatory and Earthquake Research Institute (KOERI) between October 2011 and 2012. Their findings indicated a shallow range of 4–10 km in the aftershock distribution, characterized by a low-angle thrust system. Bayrak et al. (2013) analyzed the seismogenesis and earthquake triggering during the first 40 days of the Van earthquake aftershock sequence with 2D mapping of b- and p-values, 3D mapping of b-value, and coseismic Coulomb stress modeling. They observed that the mainshock occurred in a highly stressed region and argued that the sequence comprised larger aftershocks due to large asperities within the rupture zone. Utkucu et al. (2013) calculated Coulomb stress changes before and after the 23 October 2011 Van, eastern Türkiye. According to their study, the coseismic stress changes of the background seismicity had slightly promoted stress over the rupture plane of the 2011 Van earthquake, it released a stress shadow over the Gürpınar Fault which was discussed as the source of the 7 April 1646 Van earthquake. Based on historical seismicity information, it is also discussed that the repetition of the 1646 Van earthquake would be the most likely candidate to strike the Lake Van area in the future. Spatial distribution and source mechanisms of the 2011 Van earthquake's aftershocks have been utilized to define four clusters about their relative location to the mainshock rupture. Correlations between the aftershock patterns and the coseismic Coulomb stress changes are determined by calculating the stress changes over optimally oriented and specified fault planes. It is shown that there is an apparent correlation between the mainshock stress changes and the observed spatial pattern of the aftershock occurrence. According to the calculated stress change maps, the 2011 Van earthquake decreased the stress over the GF, further delaying the successor of the 1646 Van earthquake strike. Vanacore et al. (2013) detected a deep Moho in eastern Anatolia of up to approximately 55 km and an extremely high V_P/V_S ratio (>1.85) compared to that could be associated with recent volcanism in eastern from receiver function analysis of data for the period between 2005 and 2010. In the study of Delph et al. (2015), ambient noise tomography was employed to analyze the crustal thickness and 3-D shear-wave velocities across the Anatolian Plate. The findings indicated a calculated crustal thickness of approximately 40 km. The shear-wave velocity models unveiled an average crustal Vs ranging between 3.2 and 3.5 km/s along the Eastern Anatolian Plateau, with a mantle S-wave velocity of about 4.2 km/s observed in the Lake Van region. Govers and Fichtner (2016) employed regional full-waveform tomography to visualize Anatolia's crust and uppermantle structures in their investigation. This analysis revealed the presence of ultraslow velocities (≤4.3 km/s) beneath eastern Anatolia. Notably, in eastern Türkiye, the Moho depth exhibited a range between 34 and 52 km, consistent with the conclusions drawn by Vanacore et al. (2013). According to Oruç et al. (2017) the strong negative Bouguer anomalies in Eastern Anatolian plateau have low density and relatively thick crustal root. They also suggest that the crust is thickened by the vertical loads and compressive forces up to 34–46 km. Toker et al. (2017) analyzed the source mechanisms and faulting pattern of the aftershocks in the Lake Erçek area, Eastern Anatolia, during the 2011 Van event (Mw 7.1) to drive a stress tensor acting around Lake Erçek. In their study, the focal mechanism and seismic reflection data proved that Lake Erçek was initially generated by compressional activity. Kind et al. (2015) utilized S-receiver functions in their analysis, aiming to explore variations in lithospheric thickness across the entire region of Türkiye and its surrounding areas. They employed teleseismic data to characterize seismic discontinuities between the Moho

and the discontinuity at a depth of 410 km. Their findings indicated that the Lithosphere-Asthenosphere Boundary (LAB) depth beneath the Anatolian region ranged between 80 and 100 km, whereas this depth did not change significantly when traversing the North Anatolian and East Anatolian fault zones. Çınar and Alkan (2017) studied the crustal and uppermantle structures around Lake Van by analyzing the inversion fundamental mode Rayleigh wave phase velocity dispersion curves. Their findings revealed an average shear-wave velocity in the lower crust of approximately 3.5 km/s, suggesting a potential association with volcanism. The S-wave velocity models confirmed a crust-mantle boundary at around 42 km, displaying shear velocities ranging from 3.6 to 4.2 km/s. Additionally, velocities in the uppermantle, spanning 45 to 70 km, were slower than those suggested by global models, hinting at the possible presence of hot asthenospheric material. Mahatsente et al. (2018) employed gravity models to examine the crust and uppermantle structures, aiming to understand the driving forces behind asthenospheric flow and the isostatic condition in Eastern Anatolia. They used both terrestrial and satellite-derived gravity data for their analysis. The constructed gravity models revealed notable variations in lithospheric thickness between the Anatolian and Arabian plates. Specifically, the lithospheric mantle in Eastern Anatolia exhibited a thinner profile (approximately 62–74 km) compared to the Arabian plate (approximately 84–95 km), suggesting a possibility that a portion of the Anatolian mantle lithosphere may have undergone removal through delamination. In the study of Toker and Şahin (2019), high-resolution crustal tomography beneath the tectono-magmatic lake regions (Lakes Van and Erçek) of Eastern Anatolia (Türkiye) was employed to estimate Poisson's ratio from the Vp and Vs structures. This was achieved through joint inversion analyses of Vp and Vs traveltimes, using the station records from the permanent network of Kandilli Observatory and Earthquake Research Institute (KOERI, Türkiye). The results of Poisson's ratio anomaly reveal distinct and substantial variations in different tectonic units, demonstrating prominent, continuous, and dense high Poisson's ratio anomalies in the range of 0.27 to 0.30 for the lowermost crust/the uppermost mantle beneath the regions of Lakes Van and Erçek, along with comparably low average Poisson's ratio (approximately 0.23) anomalies for the brittle crust in several local areas.

According to a Pn velocity distribution study by Hearn and Ni (1994), low Pn velocities (<7.9 km/s) beneath most of the Turkish-Iranian Plateau and high Pn velocities (>8.1 km/s) beneath the Black Sea and southern Caspian Sea. Çınar and Alkan (2017) investigated 1-D crustal structure in Eastern Anatolia by the Rayleigh wave method. Alkan et al. (2020) employed P and S wave receiver functions and their joint inversions to investigate the lithosphere beneath the Lake Van region. Utilizing approximately 600 teleseismic earthquake data, the study revealed that the V_P/V_S ratio around the east and west of Lake Van exceeded the standard value (1.73), reaching 1.85. Velocity models for the Lake Van region indicated that the thinnest Moho was identified in the east of Lake Van (approximately 42 km), while the thickest Moho was calculated in the north of Lake Van (approximately 45 km). The previous studies were either large-scale or limited to the western region west of Lake Van. The area lacks a 1-D velocity model derived from high-quality data recorded by a dense network. Aftershock sequences provide valuable information to understand the earth's crust and source properties of large earthquakes due to the large number of events occurring during a short period in a small area (Singh et al., 2012). Toker and Şahin (2022) studied on multifrequency P- and S-wave attenuation tomography models of Lake Van area (East Anatolia) by estimating coda-normalized wave spectra of 3027 local earthquakes ($2.0 < Mw < 7.1$). In the study by Toker et al. (2021), the finite source characteristics of the 2011 Van earthquake were determined by using the teleseismic waveforms to focus on the source location. This study presents the study's results on the aftershock series of the Mw = 7.1 Lake Van thrust event. A combined temporary and permanent station network recorded the aftershocks. Accurate and reliable hypocenters were obtained by applying the concept of the minimum 1-D model by Kissling (1988) and Kissling et al. (1994). The accurate hypocenters are used to estimate the seismogenic depth range and to correlate with the tectonic structures of the Lake Van region and surroundings.

2. Tectonic and geological settings

The East Anatolian High Plateau, northwestern Iran, and the Caucasus regions belong to one of the high elevation zones (average approximately 2 km) along the Alpine-Himalayan Mountain belt (Şengör and Yılmaz 1983; Jackson, 1992; Şengör et al., 2003). The region is under a compressional regime due to the collision of Arabian and Eurasian plates initiated 11 Ma ago (Şengör and Yılmaz, 1981; Şengör et al., 2003). According to GPS measurements, the northward movement of the Arabian Plate to Eurasia is about 18–20 mm/year (Reilinger et al., 2006). As seen in Figure 1, the Lake Van Basin is located east of Karlıova Triple Junction, where North Anatolian and East Anatolian Faults intersect. The Lake Van Basin is assumed to be a remnant of continental collision during the oceanic closure and subduction of the Arabian Plate beneath the Eurasian Plate (Şengör and Kidd, 1979; Dewey et al., 1986; Şaroğlu and Yılmaz, 1986) due to the north-south shortening regime where the continental collision zone between Arabia and Eurasia. The region is

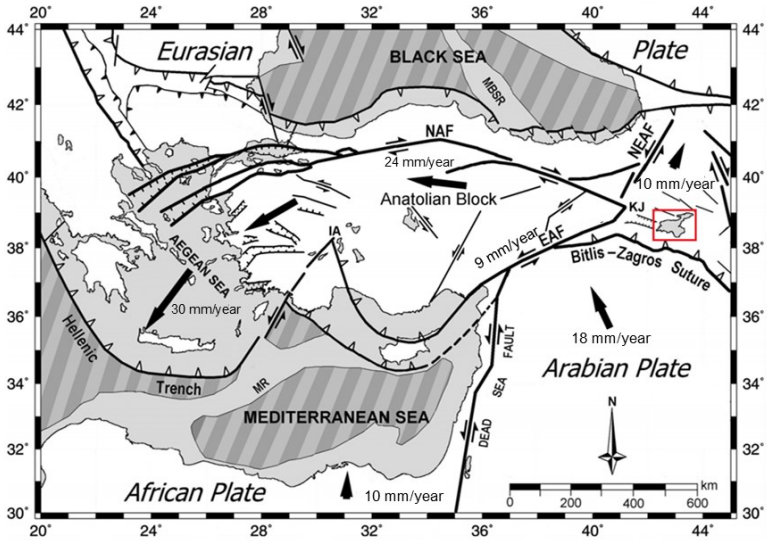

Figure 1. Simplified tectonic map of the eastern Mediterranean region modified after Gülen (1989). GPS-determined plate/block motions relative to Eurasia are shown with thick arrows, and the obtained slip rates are also given (McClusky et al., 2000). The African Plate's motion is the NUVEL-1A estimate (DeMets et al., 1990). The oceanic crusts of the Black Sea (Finetti et al., 1988) and the Mediterranean Sea (Bogdanov et al., 1994) are indicated with a striped pattern. CAF, Central Anatolian Fault; EAF, East Anatolian Fault; NAF, North Anatolian Fault; NEAF, North Eastern Anatolian Fault; IA, Isparta Angle; KJ, Karlıova Junction; MBSR, Mid-Black Sea Ridge; MR, Mediterranean Ridge (Gülen et al., 2002).

accommodated by thrust and conjugate strike-slip faults (Figure 1). According to historical and instrumental period seismic data, Lake Van is in a highly seismic area with a complex tectonic regime. The results of the focal mechanism and stress analysis solutions by Kalafat et al. (2014) also support that the 2011 Van earthquakes occurred on the reverse faulting and the seismic activity has been continuing under a compressional regime in the region.

The geology of Lake Van is seen in Figure 2. The Lake Van Basin is bounded by Quaternary volcanic in the northeast (Mount Tendürek, 3533m), in the north (Mount Süphan, 4051 m), and the west (Mount Nemrut, 2950 m) and the Bitlis-Zagros Structure Zone in the south. The southern geology of Lake Van is formed of Paleozoic metamorphic rocks called the Bitlis Massif. In Figure 2, volcanic rocks exist on the northern and western parts of Lake Neogene and Quaternary. Ophiolitic melange units are observed in the eastern Lake Van region of the Upper Cretaceous-Oligocene (Üner and Mutlu, 2019). In Lake Van, 700-m-thick sediments accumulated 600 thousand years ago (Litt et al., 2009; Stockhecke et al., 2014).

Although it was known that the eastern part of the Lake Van Basin was affected by Gürpınar, Everek, and Alaköy Faults (Koçyiğit et al., 2001), there was insufficient information regarding the recent activity of the fault in the literature until the Van earthquake happened. Evidence of an apparent surface rupture was not observed after the earthquake, and the deformation structures at the surface reflect the thrust nature with a deformation that affected approximately 8 to 12 km on land (Emre et al., 2011, 2013; Özalp et al., 2011; Özkaymak et al., 2011; Doğan and Karakaş, 2013; Koçyiğit, 2013). The Van Fault Zone is a 70-km-long, extends on E-W, northwest dipping, and approximately N70°W striking thrust fault (Figure 2) (Akyüz et al., 2011; Emre et al., 2011; Kalafat et al., 2012c; Koçyiğit, 2013; Mckenzie et al., 2016). The focal mechanism solutions of the Van earthquake aftershocks also support the region under a compressional regime that causes the reverse fault mechanism in the region (Kalafat et al., 2014). According to the stress analysis results, the compressional (P) direction of the stress axes is in the NNW/SSE direction, whereas the extensional (T) direction (ENE-WSW), which is coherent with the aftershock distribution in the region (Kalafat et al., 2014). The distribution of the aftershocks covering approximately an area of 2300 km^2 supports the presence of a rupture approximately 70 ± 10 km long (Kalafat, 2012c; Gallovic et al., 2013). Seismological studies show that the lithospheric thickness is thin in the region (Al Lazki et al., 2003; Gök et al., 2003; Keskin, 2003; Şengör et al., 2003; Lei and Zhao, 2007). During the East Anatolian Seismic Experiment

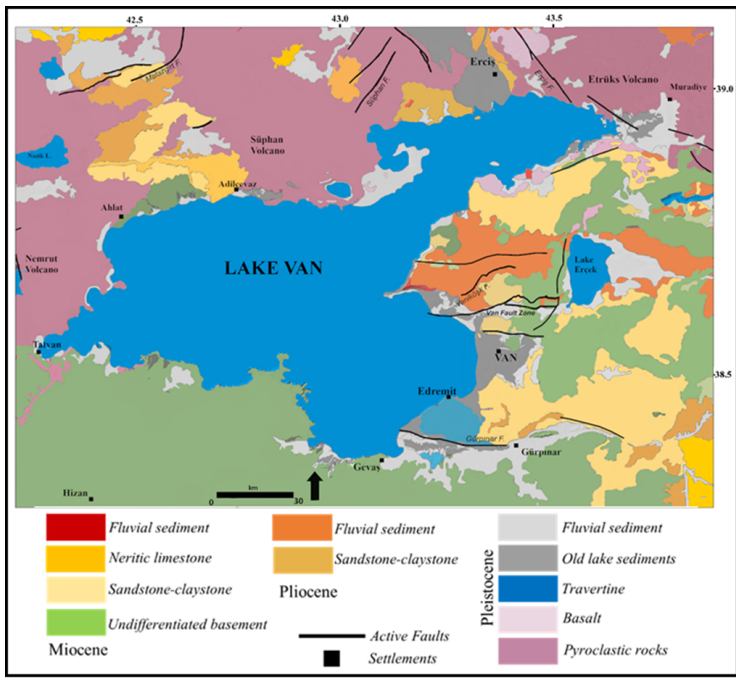

Figure 2. Geological map of Lake Van and surroundings (compiled from Senel and Ercan, 2002). Location and active fault map of the study area and digital elevation model (DEM) of Lake Van and its surroundings. Beyüzümü Fault by Ateş et al. (2007), Gürpınar Fault and Edremit Fault Zone by Özalp et al. (2016), and other active faults by Emre et al. (2013) and Selçuk et al. (2020).

(ETSE) project that covers the area on the west part of Lake Van, several researchers concluded that beneath East Anatolia, the lithospheric mantle is thin or absent (Gök et al., 2000; Al Lazki, 2003; Gök et al., 2003; Sandvol et al., 2003; Angus et al., 2006). Eastern Anatolia's crustal thickness is 45 km (Zor et al., 2003).

3. Seismic networks and data collection

Lake Van region has been monitored by the Kandilli Earthquake Research Institute (KOERI) and Disaster and Emergency Management Presidency (DEMP) permanent seismic network for a long time; however, the station distribution was not dense enough to apply a tomographic study in the region as seen in Figure 3. The 2011 Lake Van earthquake was recorded by only three seismic recordings within 200 km of the mainshock (Gülerce et al., 2012).

After the Van earthquake (Mw 7.1) on October 23rd, 2011, 10 seismic stations (eight broadband and two acceleration seismometers) were installed around Lake Van for several days to detect the aftershock sequence for 6 months. Figure 4 shows the study area with the newly installed network and existing stations. Some new network stations stayed for six months, while others were kept permanently.

The dataset is manually analyzed by using the zSacWin program developed at KOERI's Regional Earthquake and Tsunami Monitoring Center (RETMC) (Yılmazer, 2003) that is based on HYPO71 software (Lee and Lahr, 1972). The aim of using this method is to build a uniform, reliable, manually picked database and combine three different data sets as a first initial solution. VELEST program does not allow manual picking. The data set consists of KOERI, DEMP, and temporary seismic networks with a magnitude ranging between 1 and 7.2. We manually picked P- and S-wave arrival times to obtain a high-quality data set and recorded at least three stations with a minimum of 3 P-wave and 2-S wave arrivals. The data is initially analyzed by the HYPO71 location algorithm (Lee and Lahr, 1972) using a 1-D velocity model obtained by Kalafat et al. (1987) since this model is the model for routine processes at KOERI. This would be important for future comparisons of the new locations. In total, 7643 earthquakes were relocated between 23 October 2011 and 21 January 2015 within a circular epicentral distance of 350 km from the main shock. The events consisted of 48,387 P-wave arrivals and 26,913 S-wave arrival times. To get a steadier result, we relocated the events using VELEST software (Kissling et al., 1995a) in single-event mode using the velocity model (Pınar et al., 2007). Earthquake distribution is shown in Figure 5.

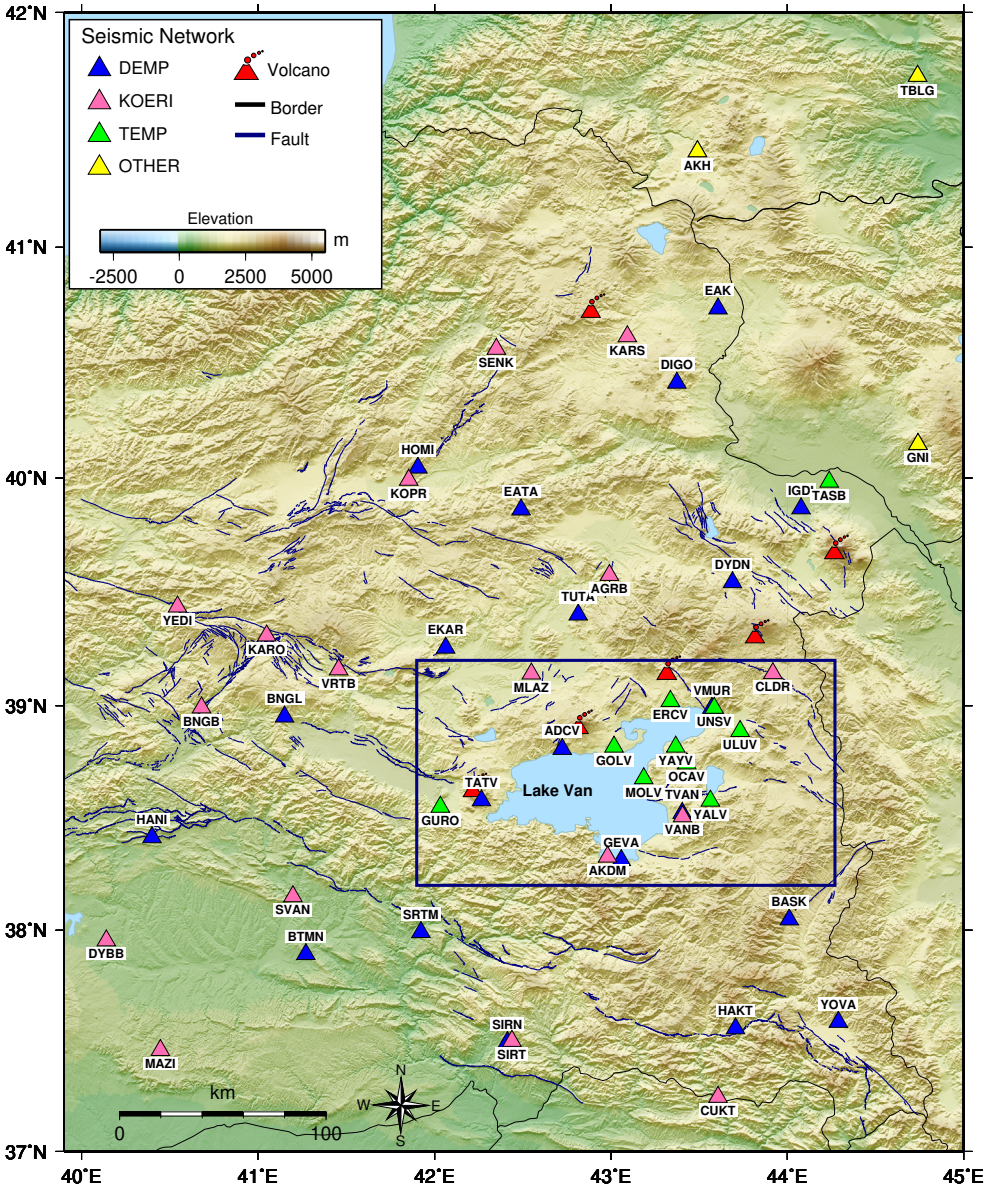

Figure 3. Station distribution map. The triangles are seismic station networks of KOERI and DEMP in Eastern Anatolia. The rectangular area is the study area selected for 1-D inversion. Location and active fault map of the study area and digital elevation model (DEM) of Lake Van and its surroundings. Beyüzümü Fault by Ateş et al. (2007), Gürpınar Fault and Edremit Fault Zone by Özalp et al. (2016), and other active faults by Emre et al. (2013), Selçuk et al. (2020).

4. The 1-D P-wave velocity model

Seismic wave traveltime is a nonlinear function of hypocentral parameters and seismic velocities sampled along the ray paths between stations and hypocenters. The dependence on seismic velocities and hypocentral parameters is the coupled hypocenter-velocity model problem (Crosson, 1976; Kissling, 1988; Thurber, 1992). However, in a standard earthquake location procedure, the velocity parameters are fixed a priori, and observed traveltimes are minimized by perturbation of hypocentral parameters (origin time, epicentral coordinates, and depth). Ignoring the coupling between hypocentral and velocity parameters during the location can cause systematic errors (Eberhart Phillips and Michael, 1993) in the hypocenter location. In addition, error estimates are strongly affected by the a priori velocity model (Kissling et al., 1995b).

Precise hypocenter locations and error estimations demand the solution of velocity and hypocentral parameters in the coupled inverse problem. The minimum

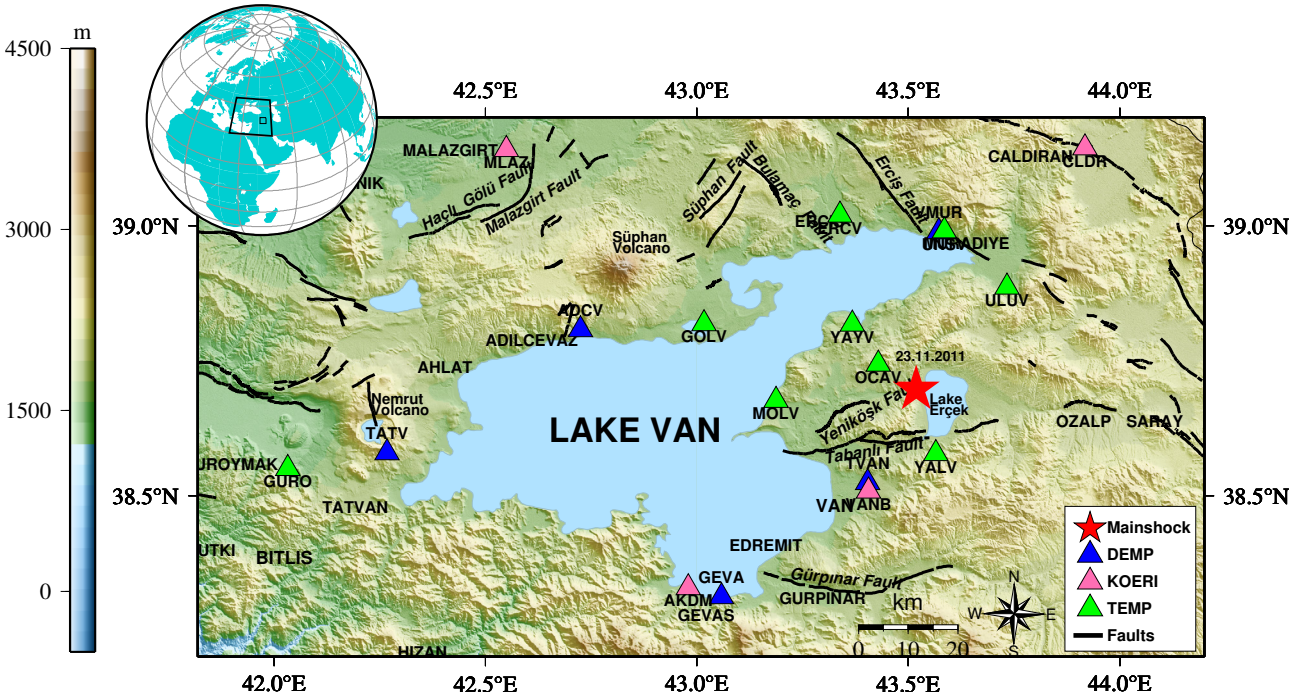

Figure 4. Study area. Map showing active faults in Lake Van, and surroundings and distribution of seismic stations (triangles). The 23 October 2011 Van earthquake is shown as the red star. Gürpınar and Edremit Fault zones are compiled from Özalp et al. (2016). Beyüzümü Fault is compiled from Ateş et al. (2007). Other faults are from Emre et al. (2013).

1-D velocity model is calculated by simultaneous inversion of hypocenter and velocity parameters by trial-and-error process (Kissling, 1988). The velocity of each layer of the minimum 1-D velocity is the weighted average of all rays within that depth (Husen et al., 1999). For lateral variations station corrections in shallow layers, station corrections are merged in the inversion process. For stations with good azimuthal ray distribution, corrections will indicate near-surface geology. Those regions with poor azimuthal station distribution station corrections in the far regions of the network contain velocity information about the shallow subsurface and linear effects of the deep structure.

To determine the study area's minimum 1-D velocity model, we used the iterative 1-D inversion algorithm, VELEST routine (Kissling et al., 1995a), that accounts for station elevation. The nonlinear problem is linearized, and the solution is obtained iteratively, whereas each iteration consists of solving the forward problem and the inverse problem at once with station corrections. Including station elevations in the inversion process allows us to trace rays to the proper positions during the forward modeling.

Data quality is essential for the success, efficiency, and accuracy of the inversion process. Before the inversion process, we relocated all events by using the velocity model (Pınar et al., 2007) running the VELEST software in single mode (Figure 6). In order to build a reliable and high-quality data set, we applied selection criteria for the data set of all events. For the inversion process, only the events that consist of a minimum of 10 P-wave arrivals with an azimuthal gap smaller than 180° were selected (Figure 6). The depth distribution of the aftershocks (Figure 7) mainly ranges from 5 to 25 km, with a maximum depth of 40 km (Figure 7).

The selected data set and seismic stations used during 1-D inversion with VELEST software consist of 1193 local events (Figure 8a). The depth distribution displays NE- SW dip of the aftershock sequence (Figure 8b) and mainshock occurring at around 6 km depth (Figures 8b and 8c). Earthquake for 1-D inversion with the mainshock, latitudinal, and longitudinal cross sections is seen in Figure 8. The earthquake depth ranges from 0 to 29 km. The zero-depth earthquakes seen in (Figure 8b) are due to the sea level height that we have chosen for the inversion. The selected stations that were used during inversion are listed in Table 1.

The initial velocity model is critical for the linearized inverse problem (Kissling, 1988; Thurber, 1992; Kissling et al., 1995a). Calculating a minimum 1-D model is a trial-and-error process starting with a wide range of velocity models as initial guesses, which allows all possible velocities to be considered. We have built 100 trials of different velocity models. P-wave velocities range between 0.5 and 4 km/s for shallow layers and 7–8.5 km/s for deep layers. Layer thicknesses were established with a constant

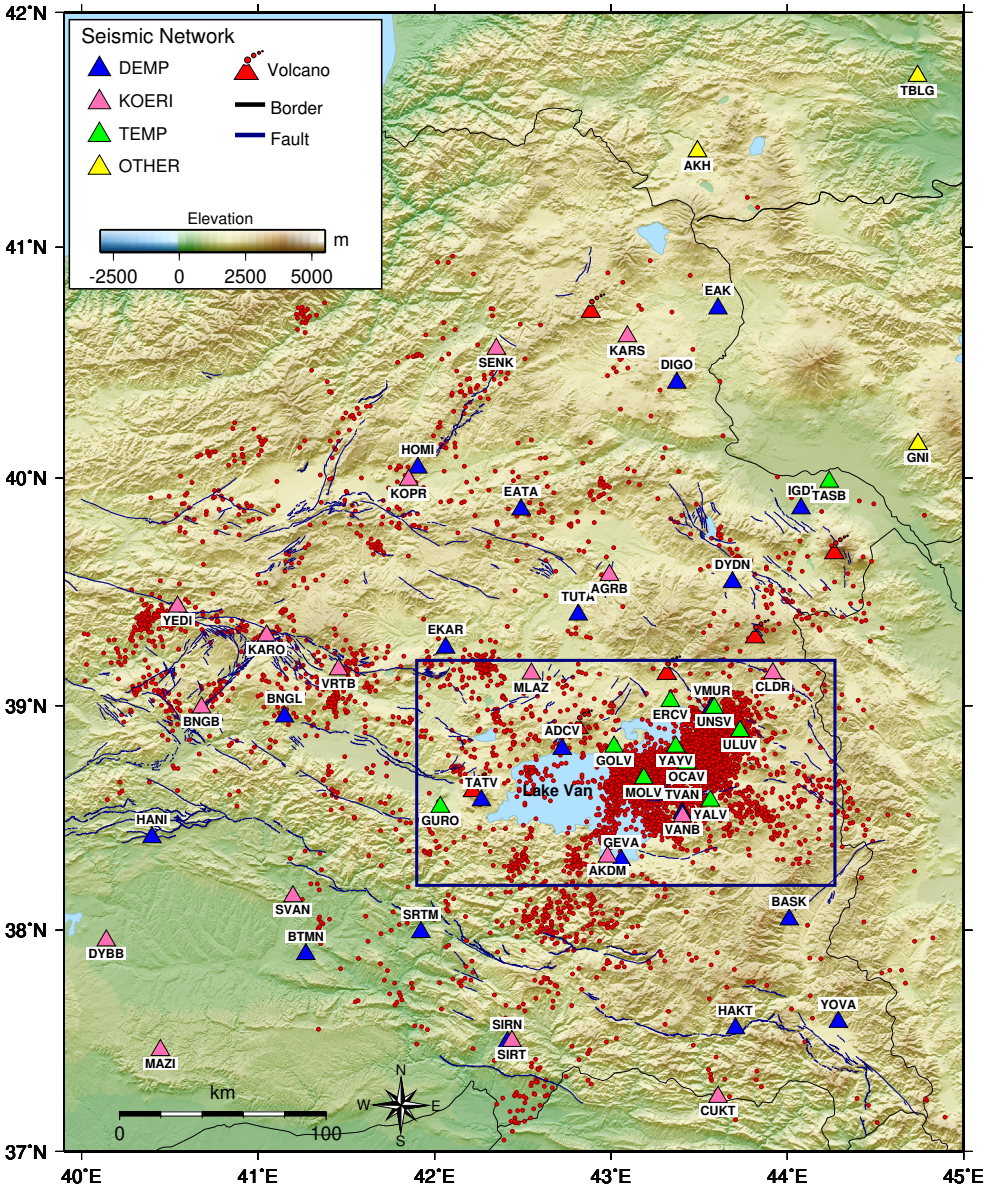

Figure 5. Earthquake and station distribution of all events after Van Earthquake with a magnitude range between 1 and 7. Earthquakes within the rectangular area are selected for this study. Dark-blue rectangular outlines the study area selected for the current study. Gürpınar and Edremit Fault zones are compiled from Özalp et al. (2015). Beyüzümü Fault is compiled from Ateş et al. (2007). Other faults are from Emre et al. (2013).

thickness of 1 km, whereas the depth range was selected from –3 km to 45 km, as shown in Figure 9.

Damping factors for the hypocentral parameters, station delays, and velocity parameters were selected to optimize parameter resolution and data misfit reduction.

An iterative simultaneous inversion was run for 100 initial models, each comprising nine iterations. We calculated velocity and hypocenter locations together with station delays. Each RMS value is obtained by the inversion. Since the lowest RMS value would give the most reliable model, we compared the RMS values obtained during the inversion. The average root mean square (RMS) of traveltime residuals of each inversion process is compared, and the 66th model with a minimum RMS of 0.18 is selected as an initial trial model for the inversion process, as seen in Figure 10.

For the next step, we ran the inversion for the selected data set (1193 events), using a damping coefficient of 0.01 for hypocentral parameters and station delays, and a damping coefficient 1.0 for velocity parameters, as

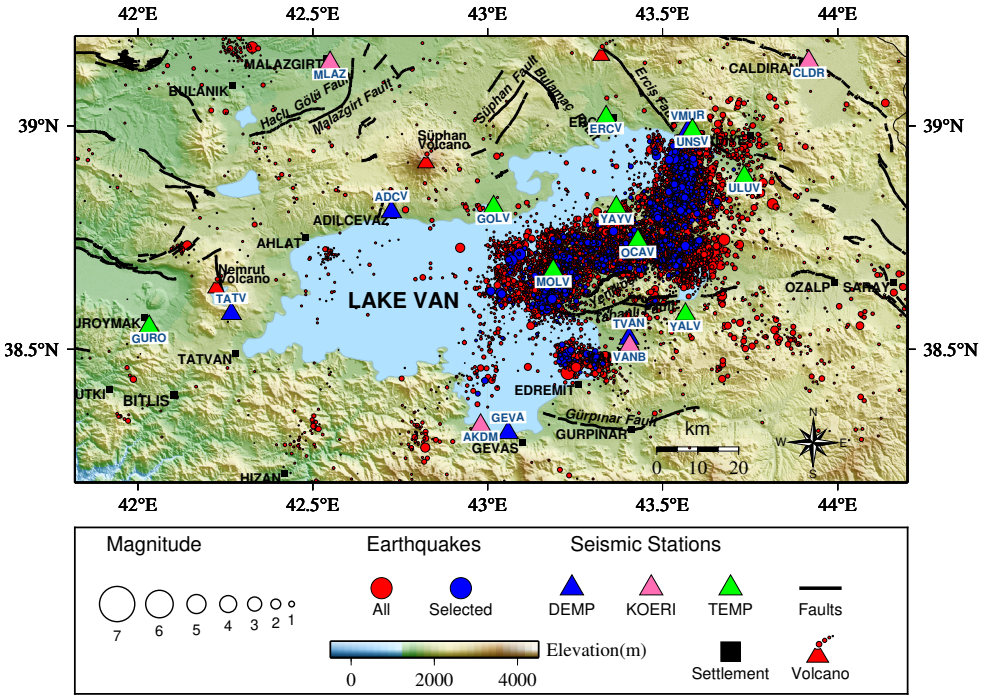

Figure 6. Relocated all and selected earthquakes within the study area; red circles 2011 Mw 7.1 Van earthquake aftershock epicenters plotted over shaded-relief topography from shuttle radar topography mission (SRTM) 1 arc-second. Blue circles are aftershock epicenters selected by certain criteria; red triangles and black squares are locations of volcanoes and cities in the area, respectively; black lines are active faults mapped in the area. Blue, pink, and green triangles are seismic networks of DEMP, KOERI, and temporary stations, respectively. Gürpınar and Edremit Fault zones are compiled from Özalp et al. (2015). Beyüzümü Fault is compiled from Ateş et al. (2007). Other faults are from Emre et al. (2013).

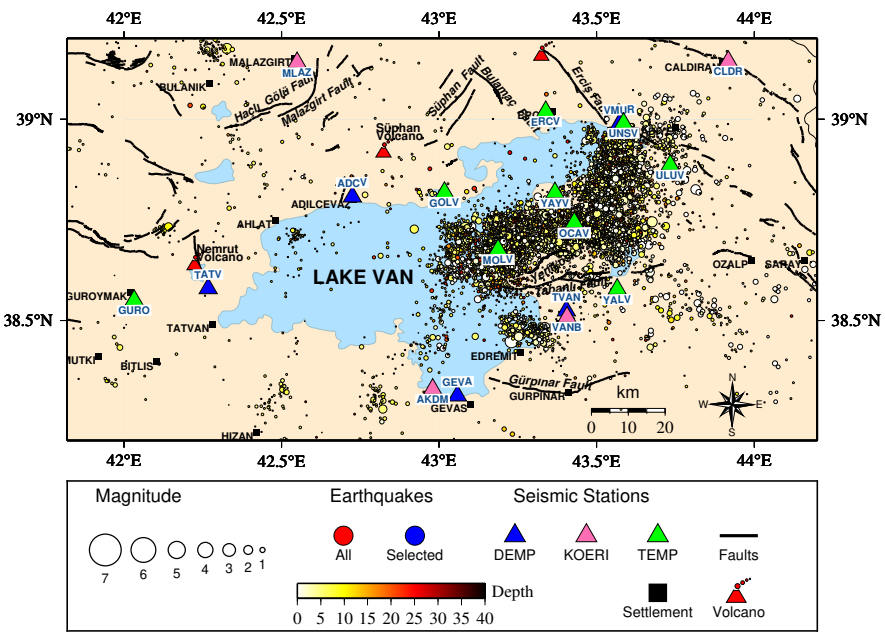

Figure 7. Relocated aftershocks of 2011 Van Earthquake (the period between 23 October 2011 and 21 January 2015). Depth distribution is shown in different colors and varying magnitude sizes. Gürpınar and Edremit Fault zones are compiled from Özalp et al. (2015). Beyüzümü Fault is compiled from Ateş et al. (2007). Other faults are from Emre et al. (2013).

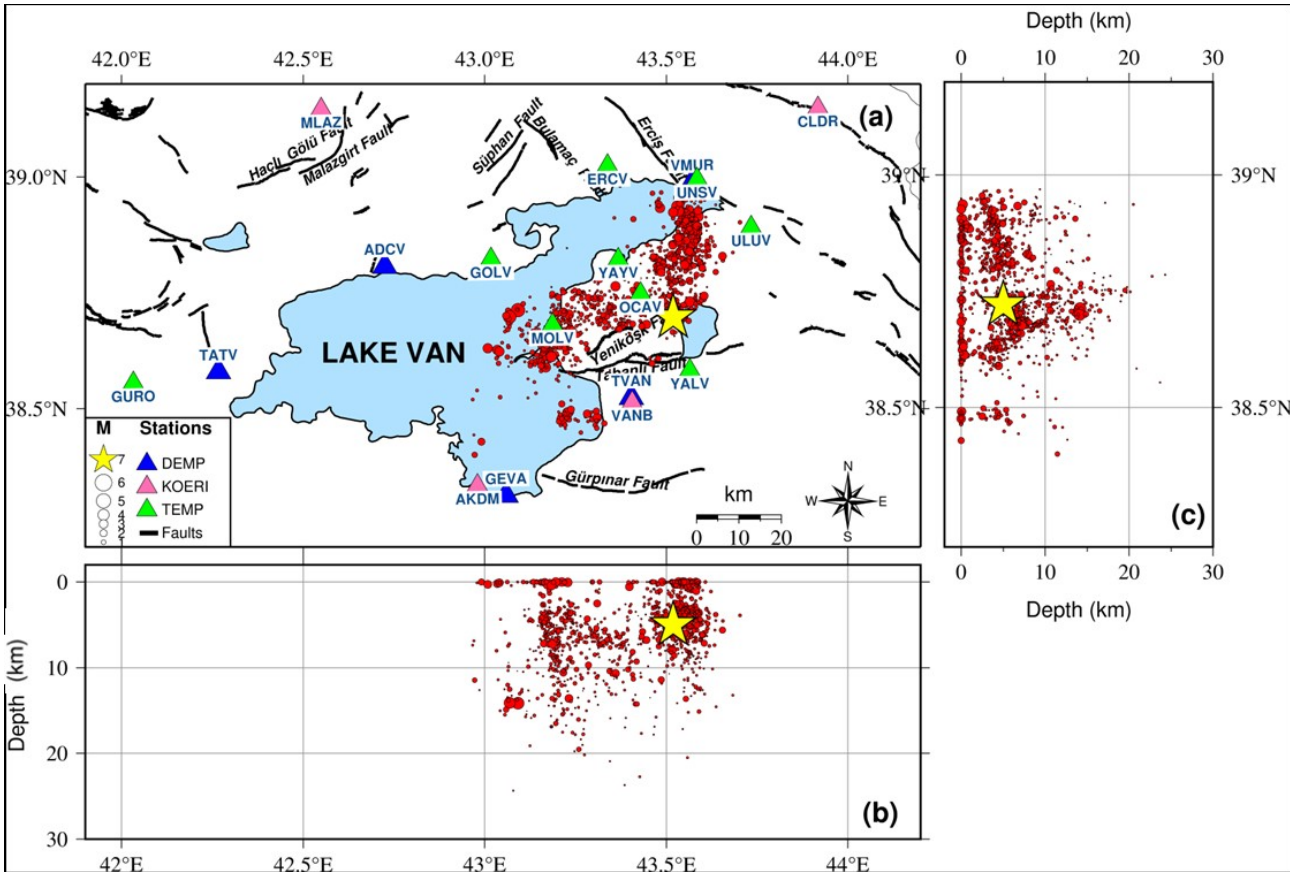

Figure 8. The selected earthquakes and stations that were used for VELEST software (a). Depth distributions are shown both by longitude (b) and latitude (c). Red circles are earthquakes, triangles are stations, and the yellow star is the mainshock epicenter. Gürpınar and Edremit Fault zones are compiled from Özalp et al. (2015). Beyüzümü Fault is compiled from Ateş et al. (2007). Other faults are from Emre et al. (2013).

Table 1. Station list.

No	Code	Latitude (degrees)	Longitude (degrees)	Elevation (m)	Location	Seismometer type	Station owner	Station opening date	Station closing date
1	ADCV	38.80	42.72	1774	Adilcevaz	Broadband	DEMP	10.28.2011	Active
2	AKDM	38.32	42.98	1662	Akdamar	Acceleration	KOERI	11.29.2012	Active
3	ERCV	39.01	43.33	1679	Erciş	Acceleration	NEW	10.25.2011	Active
4	GEVA	38.31	43.05	1672	Gevaş	Broadband	DEMP	11.02.2008	Active
5	GOLV	38.81	43.01	1663	Göldüzü	Broadband	NEW	10.26.2011	05.10.2011
6	GURO	38.55	42.03	1387	Güroymak	Broadband	NEW	10.26.2011	Active
7	MOLV	38.67	43.18	1742	Mollakasım	Broadband	NEW	10.26.2011	05.10.2011
8	OCAV	38.74	43.42	2019	Ocaklı	Broadband	NEW	10.24.2011	05.10.2011
9	TATV	38.58	42.26	1831	Bitlis	Broadband	DEMP	10.21.2006	11.12.2011
10	TVAN	38.52	43.403	2008	Van	Broadband	DEMP	10.20.2001	Active
11	ULUV	38.88	43.732	1754	Uluşar	Broadband	NEW	10.27.2011	05.10.2011
12	UNSV	38.99	43.584	1723	Ünseli	Acceleration	NEW	10.27.2011	05.10.2011
13	VANB	38.50	43.40	1227	Van	Broadband	KOERI	08.10.2000	Active
14	VMUR	38.98	43.571	1717	Van	Broadband	DEMP	11.29.2010	Active
15	YALV	38.57	43.564	1981	Yalınağaç	Broadband	NEW	10.25.2011	05.10.2011
16	YAYV	38.81	43.367	1684	Yaylıada	Broadband	NEW	10.25.2011	05.10.2011
17	TASB	39.98	44.238	844	Taşburun	Broadband	NEW	10.25.2011	Active

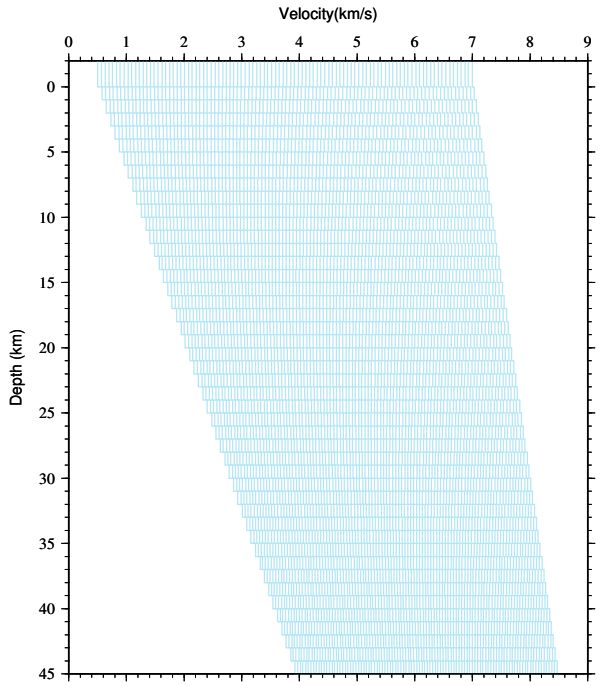

Figure 9. Initial 1-D 100 Velocity Models before inversion. P-wave velocities range between 0.5 and 4 km/s for shallow layers and 7–8.5 km/s for deep layers. Layer thicknesses are 1 km constant with a depth range from –3 km to 45 km.

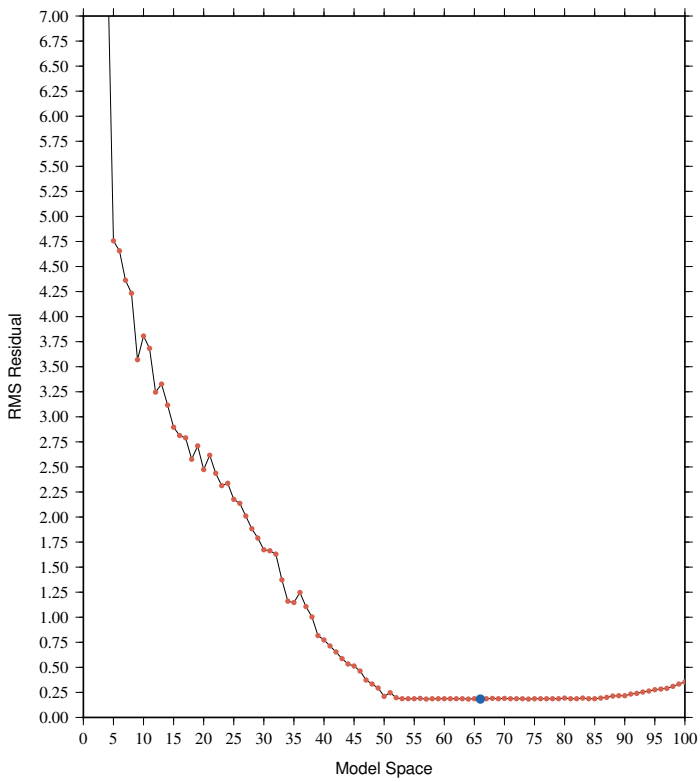

Figure 10. RMS residuals for 100 initial input velocity models. The blue dot is the minimum RMS value of 66th model.

suggested in VELEST user manual. We used nine iterations for each inversion. This step is repeated 19 times using updated velocities with new station delays and hypocenter locations. The number of layers was reduced by combining adjacent layers with similar velocities (Figure 11). This step was run until we observed locations, station delays, and velocity values did not significantly change. This trial-and-error approach allowed us to establish a reasonable geometry of the crustal model, velocity parameters, and station delays and to obtain an "updated a priori 1D model with corresponding station residuals" displayed by dark blue color in Figure 11.

We relocated all events using an updated 1-D model with station residuals with VELEST in the single-event mode. We selected 1214 events applying the same criteria defined previously. The trial-and-error approach is repeated in this step until locations, station delays, and velocity values do not significantly change. After 10 inversion steps, we obtained a "minimum 1-D model" for the region, as seen in Figure 10.

After the inversion process, the best solution is represented by a minimum 1-D velocity model. The final minimum 1-D P-wave velocity model (dark blue) and updated models (light blue) are shown in (Figure 12). The minimum 1-D model satisfies the following features: 1) Earthquake locations, station delays, and velocity values do not change significantly. 2) The RMS value of all events is reduced compared to the initial calculations, and a minimum RMS value is obtained.

5. S-wave velocity model

The usage of S-wave arrivals will provide unique information on hypocenter parameters. Gomberg et al. (1990) showed that a correctly picked S-phase recorded within approximately 1.4 times the focal depth's distance from the epicenter can serve as a potent constraint on the focal depth. Due to the frequent masking of S-arrivals by P-wave coda, there is a risk of erroneously picking the wrong S-wave arrivals. Therefore, critical quality control is necessary.

To calculate the S-wave velocity model, a new relocation process was carried out with the VELEST single-event location mode by using the final 1-D P-model P- and S-wave traveltimes and the final station corrections. New data set selection criteria are applied, and events with an azimuthal gap smaller than 180°, along with a minimum of 10 good P-wave arrivals and five S-wave arrivals, were selected. We finally checked errors in the data set by plotting P-wave arrivals and S-P wave arrivals in a Wadati diagram (Figure 13a). We eliminated the phases from the diagram to avoid the use of erroneous S-wave readings (Figure 13b). The final data set for the P-and S-wave inversion consists of

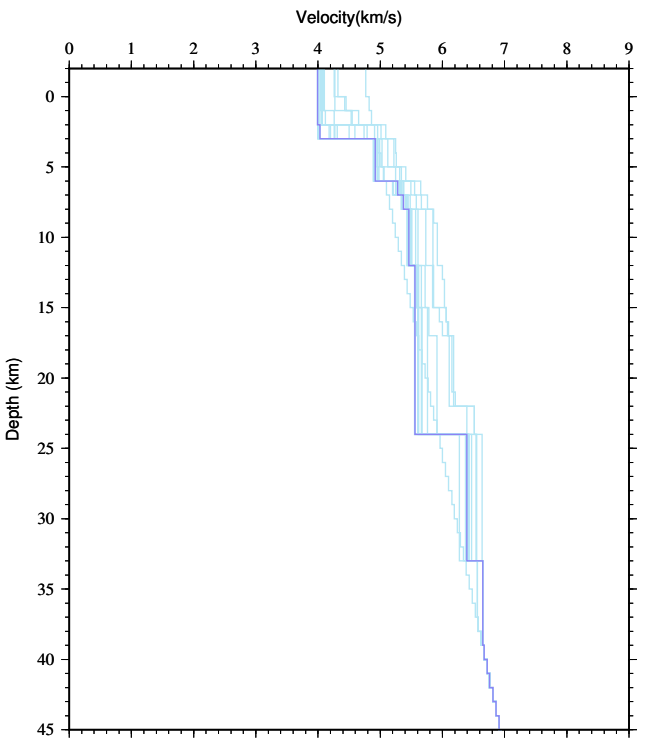

Figure 11. The 1-D P-wave velocity updated model. Dark blue lines represent the updated velocity model after several inversions.

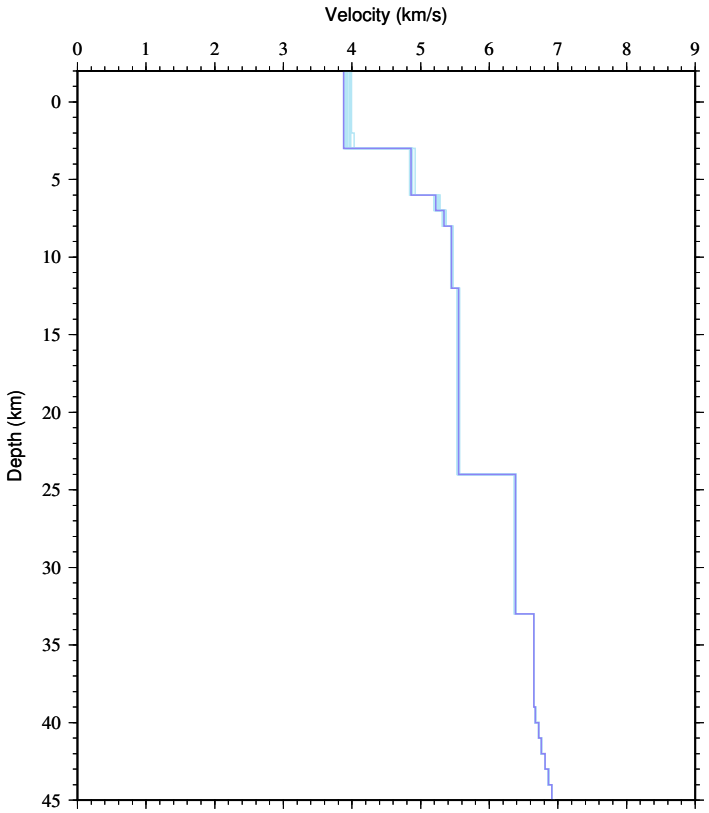

Figure 12. The final minimum 1-D P-wave velocity model (dark blue) and updated models (light blue). The final minimum 1-D model is the model with minimum RMS value.

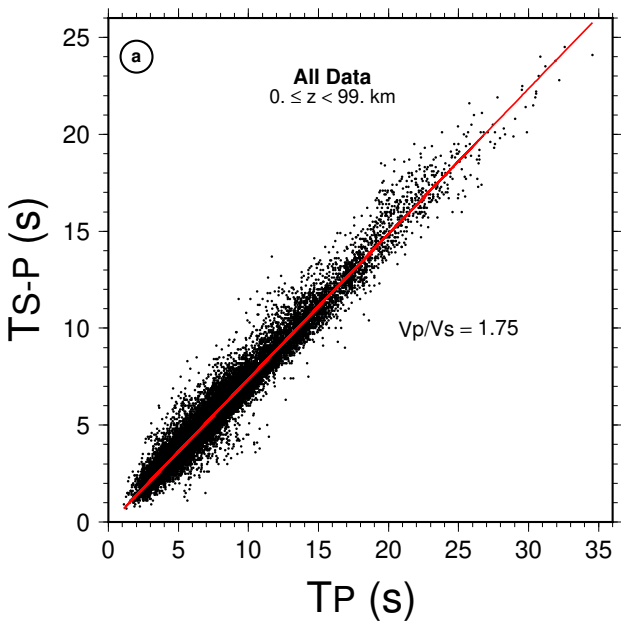

Figure 13a. Wadati diagrams before the inversion for (a) all and (b) selected data.

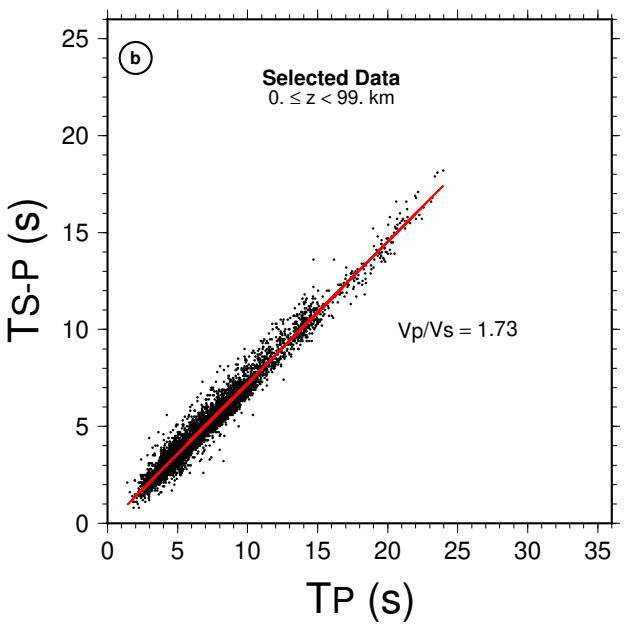

Figure 13b. Wadati diagrams after the inversion for (a) all and (b) selected data.

855 events with 9167 P-wave arrivals and 5753 S-wave arrivals. The average V_P/V_S ratio for the eliminated data before inversion is 1.73. S-phases are generally included in the location procedure by assuming a constant V_P/V_S ratio. One hundred different V_P/V_S values from 1.2 to 2.2 were utilized as initial S-wave velocity models for the joint P- and S-wave velocity inversion.

During the 1-D P and phase velocity inversion processes, the final 1-D velocity model of each iteration was kept constant by applying a high damping value for P-wave velocities. This allowed only S-wave velocity perturbations during inversion without constraints on the layers.

6. The initial and final P- and S-wave velocities, along with their corresponding V_P/V_S ratios for the initial models in Figure 14, are listed in Table 2. For depths shallower than 3 km, the V_P/V_S ratio remains close to its initial values. Below a depth of 39 km, V_P/V_S ratios could not be calculated due to a limited number of events within this depth range. Station corrections

Station delays are considered unknown parameters during the inversion process. These delays are expected to reflect the averaged basic features of local surface geology and crustal structure (Kissling, 1988; Husen et al., 1999). Early arrivals are caused by higher velocities, such as those found in volcanic rocks, whereas sedimentary rocks exhibit low velocities resulting in positive station delays (Husen et al., 2003). Station delays represent deviations from the 1-D model due to the 3-D structure of the Earth concerning a reference station (Kissling, 1988). Large models can be affected by mixed site effects, such as near-surface (sediments), and mantle phases from Moho, owing to the limited range of back azimuth at the network's edge (Diehl, 2008).

Station corrections are computed during the inversion to account for local geological changes and station elevations (Figure 15). VANB station is selected as the reference station due to its continuous recording of events towards the center of the network without extreme site conditions, resulting in less residual error. Corrections were computed relative to this reference station, with its delays (or corrections) defined as zero. Positive station correction values concerning relative to the reference station indicate local low-velocity anomalies, while negative values of station corrections correspond to high-velocity anomalies near the recording station.

In Figure 15, circles represent negative arrivals indicating higher velocities than those at reference stations, while crosses represent positive corrections

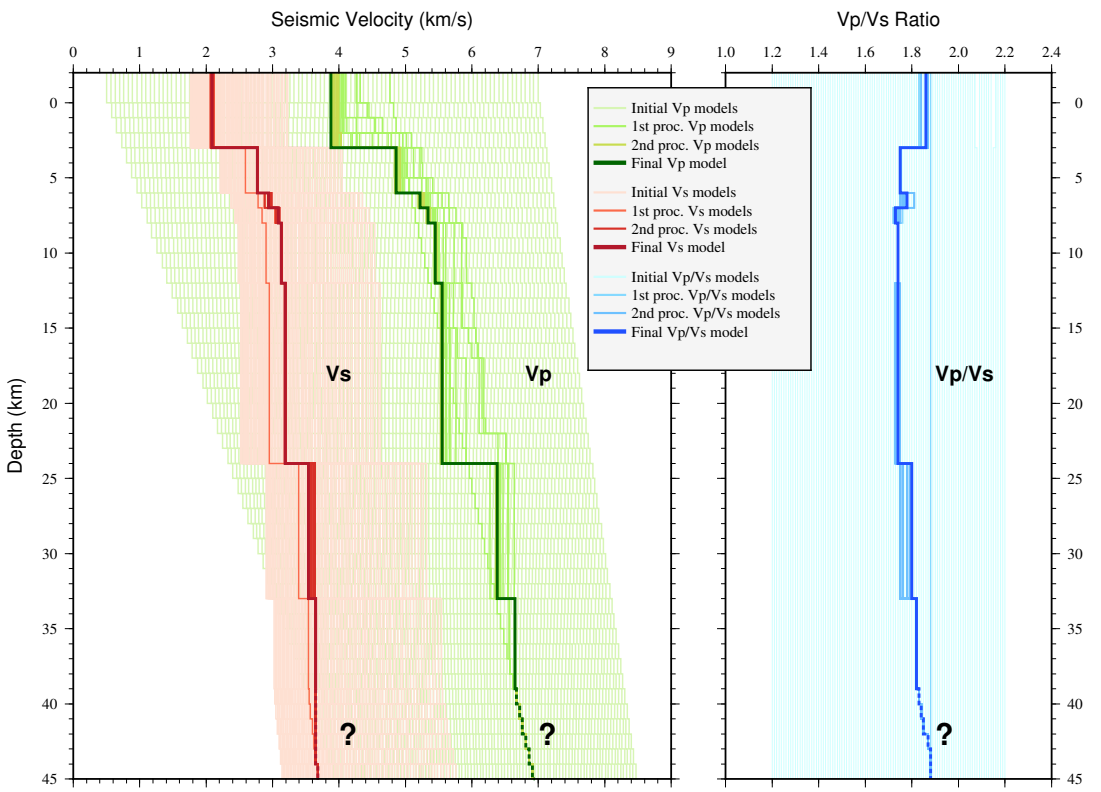

Figure 14. Initial and final P- and S-wave velocity models after velocity inversion. Dashed lines represent the layers that the inversion could not solve well.

Table 2. The 1-D P- and S-wave velocity models and V_P/V_S ratios in the Lake Van area.

Layer depth (km)	V_P (km/s)	V_S (km/s)	V_P/V_S
–3.0	3.88	2.09	1.86
3.0	4.86	2.77	1.75
6.0	5.22	2.94	1.77
7.0	5.34	3.09	1.73
8.0	5.45	3.13	1.74
12.0	5.55	3.19	1.74
24.0	6.38	3.54	1.80
33.0	6.65	3.65	1.82
39.0	6.67	3.65	1.83

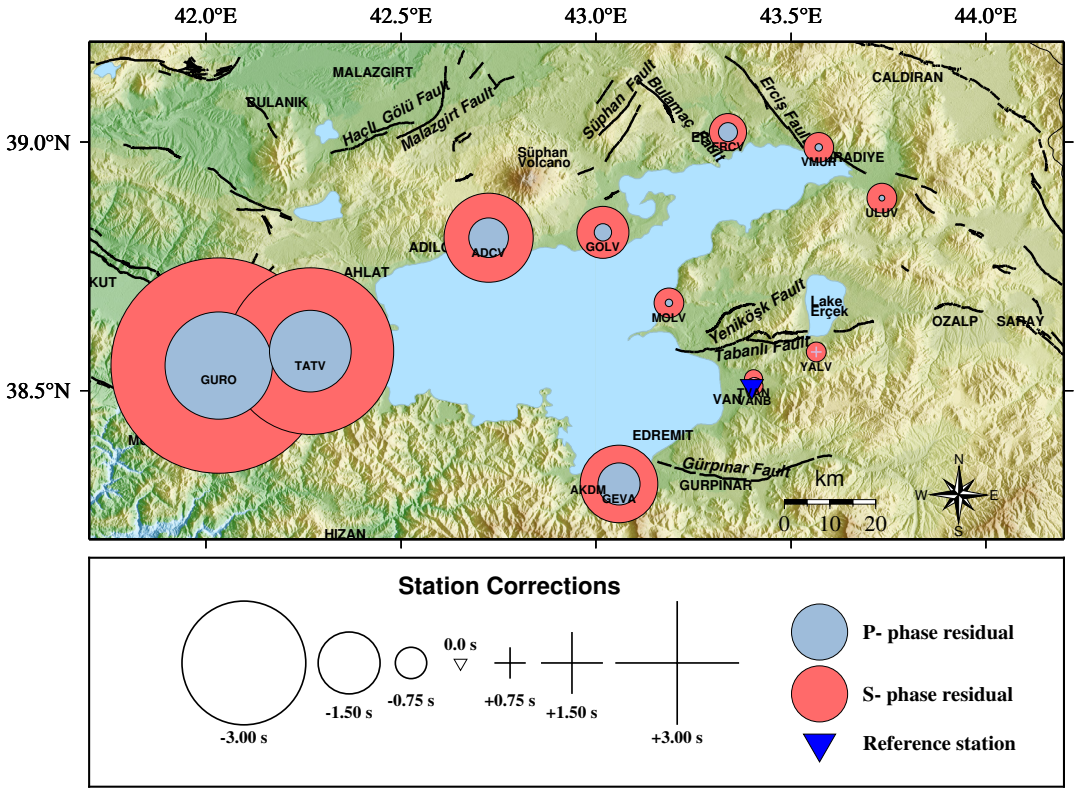

Figure 15. Final P-wave and S-wave station corrections for the minimum 1-D velocity model. The reference station (VANB) is marked by a blue triangle.

indicating lower velocities. The general pattern of station corrections indicates the consistency of the phase data. Station delays increase with distance from the reference station as the difference between modeled and unmodelled structures accumulates with longer ray paths (Husen et al., 2011). This effect can be observed in a 1-D model of the Lake Van region in the western part. The final P-wave and S-wave station corrections relative to the reference station VANB, close to the center of the network, exhibit negative delays in TATV and GURO, but show high positive delays in the eastern part. The station correction values range between –2.57 and 0.23 s.

7. Stability tests of the final 1-D P-and S-wave velocity models

To assess the stability of the final P- and S-wave minimum 1-D velocity model, two tests involving the random and systematic shifting of hypocenters were conducted. In the first test, all hypocenters were randomly shifted in all directions by 6-7 km before the velocity-hypocentral parameter inversion, aimed at identifying possible biases in their locations and evaluating the stability of the solution. Randomization was achieved using a Gaussian distribution with a zero mean. If the new 1-D velocity model yields a reliable minimum value within

the solution space, significant changes in velocity and hypocenter locations are not expected.

In the second test, all hypocenter locations were systematically shifted 10 km in East, North, and Z (depth) directions. After systematically shifting all events by 10 km, two inversions were performed: one with slightly damped (damped velocities) and one with strongly overdamped velocities (fixed velocities). The results are shown in Figures 16 and 17, respectively. Figure 18 shows the differences in focal depth, latitude, and longitude between the hypocenters obtained through inversion and those randomly shifted by 5–7 km before the inversion. We observed that all events are relocated close to their original position, indicating that the hypocenter locations obtained by inversion are not systematically biased. Two inversions were performed by fixing the velocities, with one using low damping values and the other using high damping values for velocities. In the first inversion, the minimum velocity model was allowed to invert with low damping values, while in the second inversion, a high damping value was used with fixed velocities. In Figure 17, the difference in focal depth, latitude, and longitude between the hypocenters obtained by inversion and those systematically shifted by 10 km before the inversion is seen. The blue line depicts a 10-km hypocenter shift, and the dark blue dots represent the new positions of the hypocenters after inversion.

8. Results and discussion

This paper has focused on simultaneously determining the 1-D P- and S-wave velocity models and the aftershock locations associated with the Van earthquake on October 23, 2011, in eastern Türkiye, using the traveltime inversion algorithm VELEST (Kissling et al., 1994; Akkoyunlu, 2019). The importance of this study lies in our determination of a 9-layer 1-D velocity model of Lake Van region obtained through the VELEST software, utilizing an extensive and reliable data set. We have presented a new 1-D velocity model for the region. Our study represents the first application of a 1-D velocity model covering the Lake Van region, computed through the VELEST software,

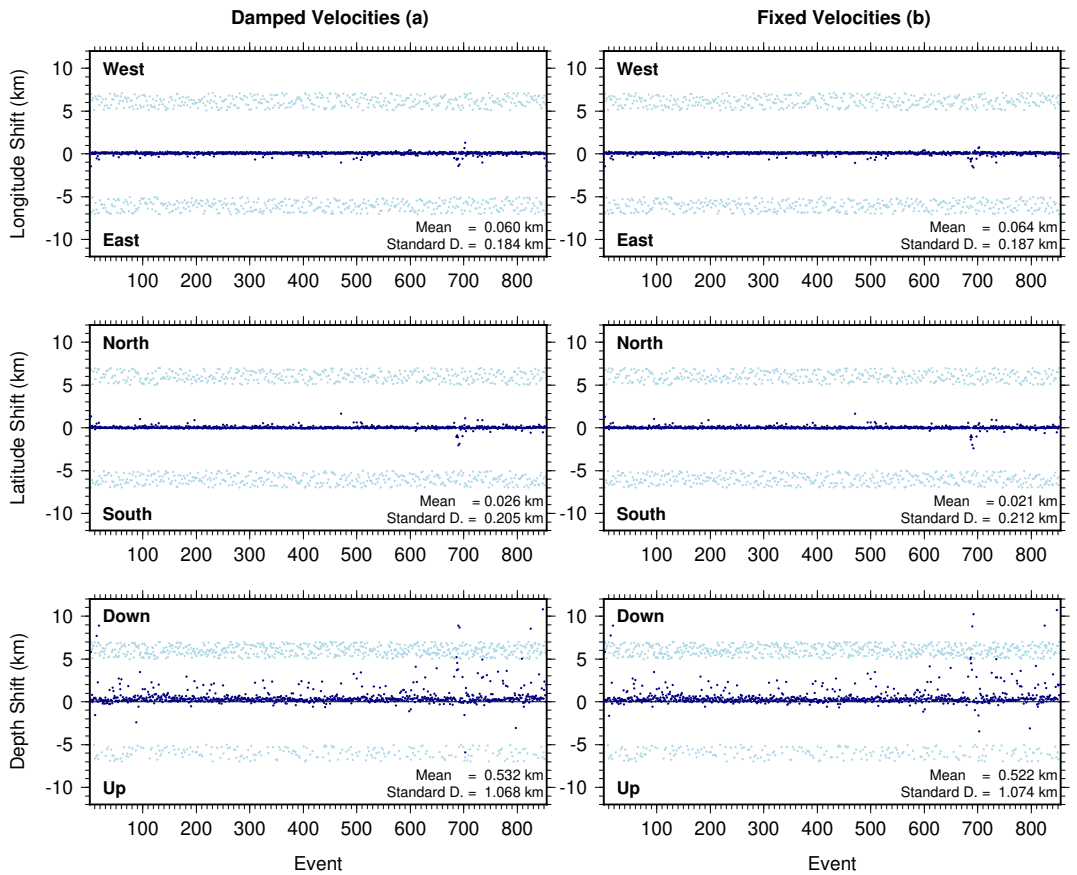

Figure 16. Results of the hypocentral random shifting test by 5–7 km with damped velocities on the left and fixed velocities on the right for minimum 1-D P-and S-wave velocity models. Light blue dots denote the random shift of hypocenter locations before inversion, and dark blue dots denote hypocenters relocated close to their original positions after the inversion.

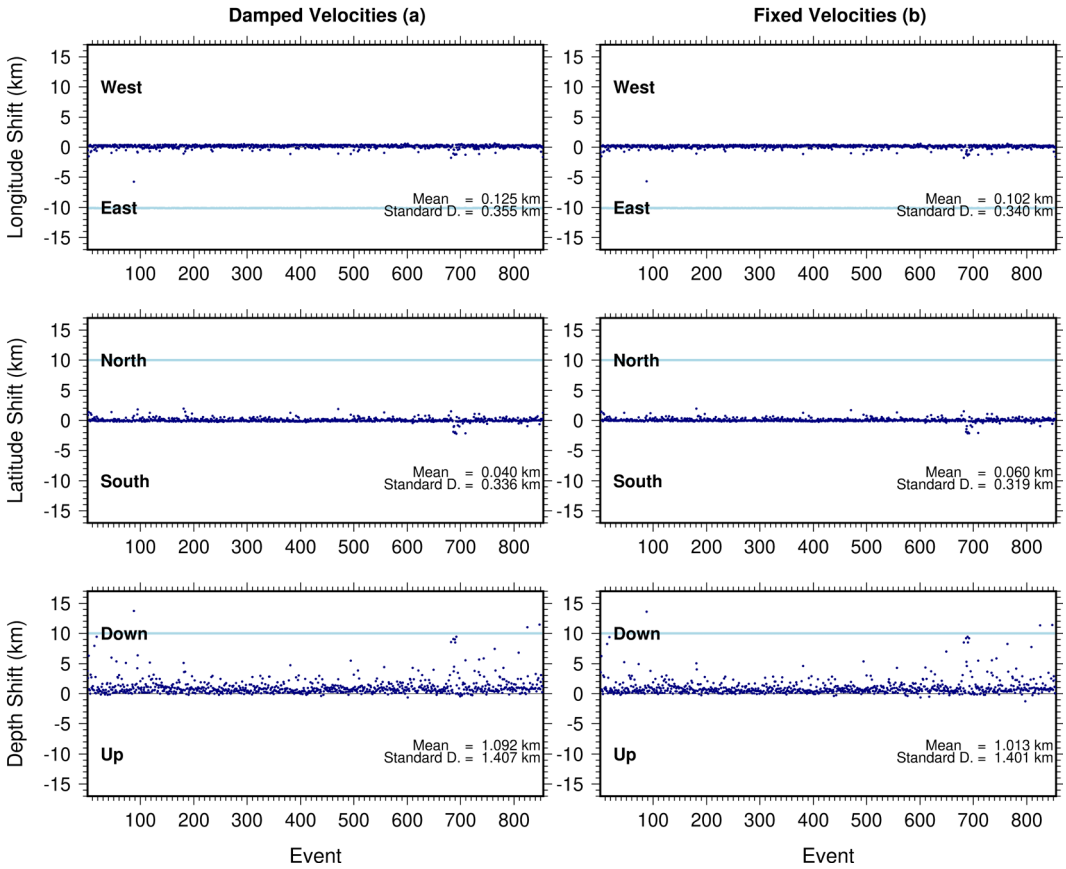

Figure 17. Results of the hypocentral systematic shifting test by 10 km with damped velocities on the left and fixed velocities on the right for minimum 1-D P-and S-wave velocity models. Light blue lines denote the systematic shift of hypocenter locations before inversion, and dark blue dots denote hypocenters relocated close to their original positions after the inversion.

utilizing an extensive dataset sourced from local stations. We have identified the first 1-D P- and S-wave velocity models with enhanced accuracy and stability. These models result in updated aftershock locations, exhibiting minimal errors in RMS values and station corrections. The 2011 Van earthquake increased the seismic activity of the eastern part of the Lake Van region, resulting in over 7000 aftershocks. The arrival times of P- and S-waves for the inversion process were determined by analyzing three distinct datasets focused on aftershocks: KOERI, DEMP, and temporary stations deployed shortly after the earthquake. Events recorded by a minimum of 10 seismic stations with an azimuthal gap of less than 180° were selected from this dataset. This improved dataset, with an enhanced azimuthal distribution, enabled the generation of stable 1-D P- and S-wave velocity models with minimal RMS value errors and precise aftershock locations. Zor et al. (2003) calculated the seismic velocities of the crustal structure of the Eastern Anatolian Plateau using receiver functions and found the shear velocity for the region to be between 3.5 and 3.8 km/s. Özacar et al. (2008) calculated the P-wave velocity (Vp) in the crust between 0 and 40 km beneath the Eastern Anatolian Plateau as 6.30 km/s in their study investigating uppermantle discontinuities. Tezel et al. (2013) investigated the Moho thickness and shear-wave velocity structure in the uppermantle beneath Türkiye using data from 120 broadband stations. The findings revealed a low-velocity layer situated at depths between 20 and 40 km, attributed to the presence of volcanic structures. Govers and Fichtner (2016) studied regional full-waveform tomography for imaging both the crust and uppermantle of Anatolia. Ultraslow velocities (≤4.3 km/s) are observed beneath parts of western and central Anatolia, and below most of eastern Anatolia. In eastern Türkiye, the Moho depth ranges between 34 and 52 km, consistent with the findings of Vanacore et al. (2013). Notable references include Zor et al. (2003), Angus et al. (2006), Özacar et al. (2008), Salah et al. (2011), Gökalp (2012), Tezel et al. (2013), Vanacore et al. (2013), Pasyanos et al. (2014), Schildgen et al. (2014), Delph et al. (2015), and Toker

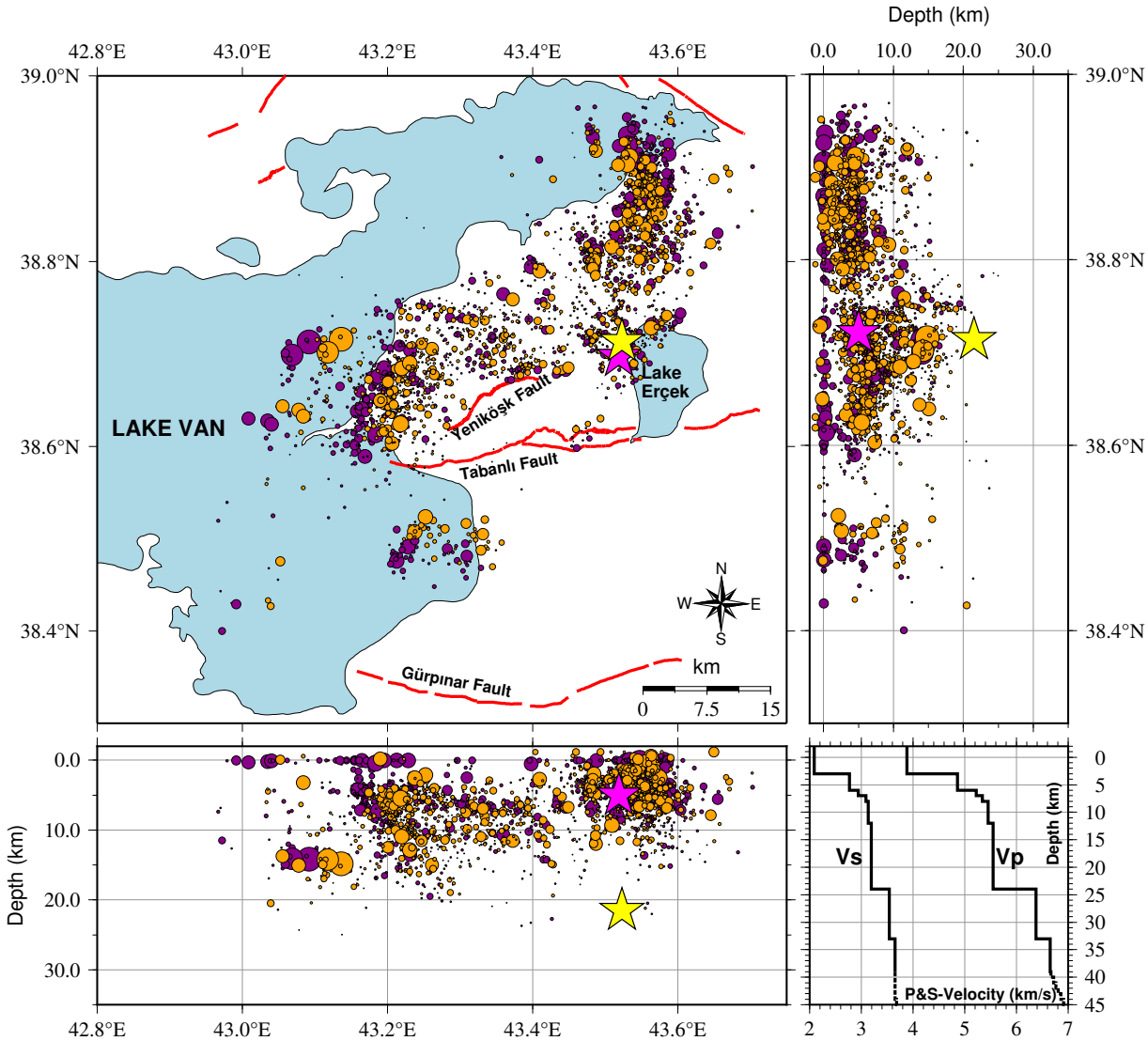

Figure 18. The final hypocenter locations of 1193 well-located events used in the P -wave and S- wave inversion. Light purple star is the first location of the Lake Van event, and purple circles are the initial location of the events. The yellow star is the new location of the Lake Van event, and the yellow circles are the latest location with the new velocity model. A latitudinal depth section is shown on the right side, and a longitudinal depth section is plotted along the bottom. The minimum 1-D models for P and S wave velocities are demonstrated in the lower right corner. The reason for the low seismicity near the new mainshock area is that the earthquake-depth distribution in Figure 18 is calculated only for the selected events (1193).

and Şahin (2019). Zor et al. (2003) calculated the seismic velocities of the crustal structure of the Eastern Anatolian Plateau using receiver functions and determined the shear velocity for the region to be between 3.5 and 3.8 km/s. In their study on uppermantle discontinuities, Özacar et al. (2008) calculated the P-wave velocity (Vp) in the crust at the depths of 0–40 km beneath the Eastern Anatolian Plateau as 6.30 km/s. Tezel et al. (2013), using data from 120 broadband stations, investigated the Moho thickness and shear-wave velocity structure in the uppermantle beneath Türkiye. Their findings revealed a low-velocity layer situated at depths between 20 and 40 km, attributed to the presence of volcanic structures. In eastern Türkiye, the Moho depth varies between 34 and 52 km, consistent with the findings of Vanacore et al. (2013).

Govers and Fichtner (2016) conducted a study on regional full-waveform tomography to image the crust and uppermantle of Anatolia. They observed ultraslow velocities (≤ 4.3 km/s) beneath parts of western and central Anatolia, as well as beneath most of eastern Anatolia. Oruç and Sönmez (2017) investigated the lithospheric structure of Eastern Anatolia and its adjacent areas, encompassing

the northern portion of the Arabian platform. Through a comprehensive analysis and modelling of Bouguer anomalies, their findings indicate that the average depths of key geological features in the study area are constrained as follows: the volcano-sedimentary layer at 7 km and the Moho depth at 39 km. The outcomes of this study closely align with the findings of the referenced investigation. Specifically, in our study, we repositioned the mainshock of the 2011 Van earthquake, adjusting its initially recorded depth range from 6-7 km to a revised depth of 21 km. This finding aligns with a coseismic surface deformation analysis conducted through interferometric synthetic aperture radar (InSAR), indicating the potential for rupture down to a depth of 25 km within the middle crust. This affirmation underscores that the Turkish–Iranian Plateau in this region possesses sufficient strength to experience rupture in large earthquakes despite extensive volcanism with elevated crustal temperatures and an unusually hot uppermost mantle, as noted by Fielding et al. (2013).

9. Conclusion

The analysis reveals that the newly established 1-D velocity model for Lake Van includes an upperlayer of the volcano-sedimentary basin around 6 km in thickness, exhibiting P-wave velocities ranging from 3.88 km/s to 4.86 km/s (see Table 2). Between depths of 6 km and 12 km, there is a gradual increase in velocity, ranging from 5.22 km/s to 5.55 km/s at 12 km. These values align with seismic velocities commonly associated with the crystalline uppercrust. At depths of 12 km and 24 km, there is a notable change in Vp seismic velocities, ranging from 5.55 km/s to 6.38 km/s. Between depths of 24 km and 39 km, there is a gradual increase in seismic velocities, ranging from 6.38 km/s to 6.67 km/s. Additionally, the volcano-sediment thickness spans from 0 to 6 km, aligning with values comparable to the global sediment map determined by seismic data (Laske et al., 2013). Our observations reveal a Moho depth of approximately 39 km, a measurement consistent with the documented range of crustal thicknesses in Eastern Anatolia. Previous studies employing receiver function and seismic tomography methods have reported crustal thicknesses spanning from 30 to 55 km in this region. The computed station corrections and the depth distribution of the new aftershock locations, derived from the updated crustal velocity model, validate the improvement in the accuracy of aftershock locations (Figure 18). Our analysis led to the conclusion that the seismogenic zone in this region does not extend beyond a depth of 25 km. After conducting numerous tests and trial solutions, a 1-D S-wave velocity model was obtained by optimizing the V_P/V_S ratio (Table 2). In the uppermost layer, the high values may suggest the presence of fluids, while the deeper high V_P/V_S ratios may be attributed to the influence of magma. For a further analysis of V_P/V_S ratios, other complementary data and analyses, such as 3-D seismic tomography studies, may be necessary to obtain. The main contribution of our study is the establishment of a reliable 1-D velocity model of the Lake Van region. This model is essential for improving the accuracy of earthquake location assessments. The recently developed 1-D velocity model will enable the determination of accurate earthquake locations in this region and serve as a foundational velocity model for future 3-D seismic tomography studies.

Acknowledgments

The equipment and data collection for this research are supported by the Boğaziçi University Research Fund within the scope of project BAP/SRP 6671. We would like to thank the Boğaziçi University Research Fund Commission and its members. Many figures were plotted using GMT (https://www.generic-mapping-tools.org/) (Wessel et al., 2013; Wessel and Smith, 1998) and GIMP software. This article is extracted from M. Feyza Akkoyunlu's doctorate dissertation, "Three-dimensional velocity structure and seismotectonic properties of Lake Van and its surroundings," supervised by Prof. Dr. Bülent Oruç (Ph.D. Dissertation, Kocaeli University, Kocaeli, Türkiye, 2019). We express our gratitude to the anonymous referees for their valuable feedback and insightful comments on our work.

Funding

No funding was received for conducting this study.

Contribution of authors

Mehveş Feyza Akkoyunlu: Conceptualization, methodology, writing, visualization, software. Bülent Kaypak: Methodology, investigation, visualization, software, writing.

Bülent Oruç: Investigation, writing. Doğan Kalafat: Data providing, equipment installation. All authors reviewed the manuscript.

Conflict of interest

The authors have no competing interests relevant to the content of this article to declare.

Data citation

We used data from KOERI (Kandilli Observatory and Earthquake Research Institute, Boğaziçi University (1971) and Republic of Türkiye Prime Ministry Disaster and Emergency Management Authority Presidential of Earthquake Department and data from the network funded by Boğaziçi University Research Fund project number BAP/SRP 6671.

References

Akkoyunlu MF (2019). Van Gölü ve Civarının Üç Boyutlu Hız Yapısı ve Sismotektonik Özellikleri. Unpublished PhD, Kocaeli University, Kocaeli, Türkiye (in Turkish).

Akyüz S, Zabcı C, Sançar T (2011). Preliminary report on the 23 October 2011 Van earthquake. Faculty of Mines, İstanbul Technical University, İstanbul.

Alkan H, Çınar H, Oreshin S (2020). Lake Van (Southeastern Türkiye) experiment: receiver function analyses of lithospheric structure from teleseismic observations. Pure and Applied Geophysics, 177: 3891–3909. https://doi.org/10.1093/gji/ggs075

Al Lazki AI, Seber D, Sandvol E, Turkelli N, Mohamad R et al. (2003). Tomographic Pn velocity and anisotropy structure beneath the Anatolian Plateau (Eastern Turkey) and The surrounding regions. Geophysical Research Letters 30 (24): 8043. https://doi.org/10.1029/2003Gl017391

Al Lazki AI, Sandvol E, Seber D, Barazangi M, Turkelli N et al. (2004). Pn tomographic imaging of mantle lid velocity and anisotropy at the junction of the Arabian, Eurasian, and African plates. Geophysical Journal International, 158 (3): 1024-1040. https://doi.org/10.1111/j.1365-246X.2004.02355.x

Angus DA, Wilson DC, Sandvol E, Ni JF (2006). From S-wave receiver functions, the lithospheric structure of the Arabian and Eurasian collision zone in eastern Turkey. Geophysical Journal International, 166 (3): 1335-1346. https://doi.org/10.1111/j.1365-246X.2006.03070.x

Ateş S, Mutlu G, Özerk OC, Çiçek İ, Karakaya Gülmez F et al. (2007). Van İlinin yerbilim verileri. MTA Genel Müdürlüğü, Rapor No: (10961): 158.

Bayrak Y, Yadav RBS, Kalafat D, Tsapanos TM, Çınar H et al. (2013). Seismogenesis and earthquake triggering during the Van (Turkey) 2011 seismic sequence. Tectonophysics 601: 163–176. https://doi.org/10.1016/j.tecto.2013.05.008

Crosson RS (1976). Crustal structure modeling of earthquake data: 1. Simultaneous least squares estimation of hypocenter and velocity parameters. Journal of Geophysical Research, 81 (17): 3036-3046. https://doi.org/10.1029/JB081i017p03036

Çınar H, Alkan H (2017). Crustal S-wave structure around the Lake Van region (eastern Turkey) from interstation Rayleigh wave phase velocity analyses. Turkish Journal of Earth Sciences, 26: 73-90. https://doi.org/10.3906/yer-1605-13

Delph JR, Zandt G, Beck SL (2015). A new approach to obtaining a 3D shear wave velocity model of the crust and upper mantle: An application to Eastern Turkey. Tectonophysics, 665: 92-100. https://doi.org/10.1016/j.tecto.2015.09.031

Dewey JF, Hempton MR, Kidd WSF, Şaroğlu F, Şengör AMC (1986). Shortening of continental lithosphere: the neotectonics of Eastern Anatolia young collision zone. In "Collision Tectonics", eds. M.P. Coward and A.C. Ries. Geological Society Special Publications 19. London. 3-36. https://doi.org/10.1144/GSL.SP.1986.019.01.01

Diehl T (2008). 3-D seismic velocity models of the Alpine crust from local earthquake tomography (Doctoral dissertation, ETH Zurich).

Doğan B, Karakaş A (2013). Geometry of co-seismic surface ruptures and tectonic meaning of the 23 October 2011 Mw 7.1 Van earthquake (East Anatolian Region, Turkey). Journal of Structural Geology, 46: 99-114. https://doi.org/10.1016/j.jsg.2012.10.001

Eberhart Phillips D, Michael AJ (1993). Three-dimensional velocity structure, seismicity, and fault structure in the Parkfield region, central California. Journal of Geophysical Research: Solid Earth, 98 (B9): 15737-15758. https://doi.org/10.1029/93JB01029

Emre Ö, Duman TY, Özalp S, Elmacı H (2011). 23 Ekim 2011 Van Depremi Saha Gözlemleri Ve Kaynak Faya İlişkin Ön Değerlendirmeler General Directorate of Mineral Research and Exploration, Ankara, Türkiye (Report in Turkish).

Emre Ö, Duman TY, Özalp S, Elmacı H, Olgun Ş et al. (2013). Active fault map of Turkey (scale: 1/250000). Ankara: General Directorate of Mineral Exploration and Research (MTA).

Fielding EJ, Lundgren PR, Taymaz T, Yolsal Çevikbilen S, Owen SE (2013). Fault-slip source models for the 2011 M 7.1 Van earthquake in Turkey from SAR interferometry, pixel offset tracking, GPS, and seismic waveform analysis. Seismological Research Letters, 84 (4): 579-593. https://doi.org/10.1785/0220120164

Gallovic F, Ameri G, Zahradnik J, Jansky J, Plicka V et al. (2013). Fault Process and Broadband Ground-Motion Simulations of the 23 October 2011 Van (Eastern Turkey) Earthquake. Bulletin of the Seismological Society of America, 103 (6): 1-15 https://doi.org/10.1785/0120130044

Gomberg JS, Shedlock KM, Roecker SW (1990). The effect of S-wave arrival times on the accuracy of hypocenter estimation. Bulletin of the Seismological Society of America, 80 (6A): 1605-1628. https://doi.org/10.1785/BSSA08006A1605

Govers R, Fichtner A (2016). Signature of slab fragmentation beneath Anatolia from full-waveform tomography. Earth and Planetary Science Letters, 450: 10-19. https://doi.org/10.1016/j.epsl.2016.06.014

Gök R, Türkelli N, Sandvol E, Seber D, Barazangi M (2000). Regional wave propagation in Turkey and surrounding regions. Geophysical Research Letters, 27 (3): 429-432. https://doi.org/10.1029/1999GL008375

Gök R, Sandvol E, Turkelli N, Seber D, Barazangi M (2003). Sn attenuation in the Anatolian and Iranian plateau and surrounding regions. Geophysical Research Letters 30. https://doi.org/10.1029/2003GL018912

Gökalp H (2012). Tomographic imaging of the seismic structure beneath the east Anatolian Plateau, eastern Turkey. Pure and Applied Geophysics, 169: 1749-1776. https://doi.org/10.1007/s00024-011-0432-x

Gülerce Z, Çetin KÖ, Yılmaz MT, Huvaj Sarıhan N, Türkoğlu M (2012). 23 October 2011 Van-Tabanlı Earthquake (Mw=7.1) Geotechnical Field Observations. In: The 10th International Congress on Advances in Civil Engineering; Ankara, Türkiye.

Hearn TM, Ni JF (1994). Pn velocities beneath continental collision zones: the Turkish-Iranian Plateau. Geophysical Journal International, 117 (2): 273-283. https://doi.org/10.1111/j.1365-246X.1994.tb03931.x

Husen S, Kissling E, Flueh E, Asch G (1999). Accurate hypocentre determination in the seismogenic zone of the subducting Nazca Plate in northern Chile using a combined on-/offshore network. Geophysical Journal International, 138 (3): 687-701. https://doi.org/10.1046/j.1365-246x.1999.00893.x

Husen S, Kissling E, Deichmann N, Wiemer S, Giardini D et al. (2003). Probabilistic earthquake location in complex three-dimensional velocity models: Application to Switzerland. Journal of Geophysical Research: Solid Earth, 108(B2). https://doi.org/10.1029/2002JB001778

Husen S, Hardebeck J (2010). Earthquake location accuracy. CORSSA. https://doi.org/10.5078/corssa-55815573

Husen S, Kissling E, Clinton JF (2011). Local and regional minimum 1D models for earthquake location and data quality assessment in complex tectonic regions: application to Switzerland. Swiss Journal of Geosciences, 104 (3): 455-469. https://doi.org/10.1007/s00015-011-0071-3

Jackson J (1992). Partitioning of strike-slip and convergent motion between Eurasia and Arabia in eastern Turkey and the Caucasus. Journal of Geophysical Research: Solid Earth, 97 (B9): 12471-12479. https://doi.org/10.1029/92JB00944

Kalafat D, Gürbüz C, Üçer SB (1987). Batı Türkiye'de Kabuk ve Üst Manto Yapısının Araştırılması. Deprem Araştırma Bülteni, Sayı 59: 43-64 (in Turkish).

Kalafat D, Suvarikli M, Ogutcu Z, Kekovalı K, Yılmazer M et al. (2012c). A recent example of continent-continent collision: October 23, 2011 Van Earthquake (Mw=7.2): Southeastern Turkey. In: American Geophysics Union AGU 2012 Fall Meeting, S51B-2420: 3-7 December 2012, San Francisco, CA, USA.

Kalafat D, Kekovalı K, Akkoyunlu F, Ögütçü Z (2014). Source mechanism and stress analysis of 23 October 2011 Van Earthquake (Mw= 7.1) and aftershocks. Journal of Seismology, 18 (3): 371-384. https:// doi.org/10.1007/s10950-013-9413-0

Kandilli Observatory and Earthquake Research Institute, Boğaziçi University. (1971). Boğaziçi University Kandilli Observatory and Earthquake Research Institute [Data set]. International Federation of Digital Seismograph Networks. https://doi.org/10.7914/SN/KO

Keskin M (2003). Magma generation by slab steepening and breakoff beneath a subduction-accretion complex: An alternative model for collision-related volcanism in Eastern Anatolia, Turkey. Geophysical Research Letters, 30 (24). https://doi.org/10.1029/2003GL018019

Kind R, Eken T, Tilmann F, Sodoudi F, Taymaz T et al. (2015). Thickness of the lithosphere beneath Turkey and surroundings from S-receiver functions. Solid Earth, 6: 971–984. https://doi.org/10.5194/se-6-971-2015

Kissling E (1988). Geotomography with local earthquake data. Reviews of Geophysics, 26 (4): 659-698. https://doi.org/10.1029/RG026i004p00659

Kissling E, Ellsworth WL, Eberhart Phillips D, Kradolfer U (1994). Initial reference models in local earthquake tomography. Journal of Geophysical Research: Solid Earth, 99 (B10): 19635-19646. https://doi.org/10.1029/RG026i004p00659

Kissling E, Kradolfer U, Maurer H (1995a). VELEST Version 3.1 User's Guide: Short Introduction. Institute of Geophysics and Swiss Seismological Service, ETH, Zurich.

Kissling E, Solarino S, Cattaneo M (1995b). Improved seismic velocity reference model from local earthquake data in Northwestern Italy. Terra Nova, 7 (5): 528-534. https://doi.org/10.1111/j.1365-3121.1995.tb00554.x

Koçyiğit A, Yilmaz A, Adamia S, Kuloshvili S (2001). Neotectonics of East Anatolian Plateau (Turkey) and Lesser Caucasus: implication for the transition from thrusting to strike-slip faulting. Geodinamica Acta, 14 (1-3): 177-195. https://doi.org/10.1080/09853111.2001.11432443

Koçyiğit A (2013). New field and seismic data about the intraplate strike-slip deformation in Van region, East Anatolian plateau, E. Turkey. Journal of Asian Earth Sciences, 62, 586-605. https://doi.org/10.1016/j.jseaes.2012.11.008

Laske G, Masters G, Ma Z, Pasyanos M (2013). Update on CRUST1.0—A 1-degree global model of Earth's crust. Geophysical Research Abstracts 15: 2658.

Lee WHK, Lahr JC (1972). HYPO71: A computer program for determining hypocenter, magnitude, and first motion pattern of local earthquakes (No. 72-224). US Geological Survey.

Lei J, Zhao D (2007). Teleseismic evidence for a break-off subducting slab under Eastern Turkey. Earth and Planetary Science Letters, 257 (1-2): 14-28. https://doi.org/10.1016/j.epsl.2007.02.011

Litt T, Krastel S, Sturm M, Kipfer R, Örcen S et al. (2009). 'PALEOVAN', International Continental Scientific Drilling Program (ICDP): site survey results and perspectives. Quaternary Science Reviews, 28 (15-16): 1555-1567. https://doi.org/10.1016/j.quascirev.2009.03.002

Mahatsente R, Onal G, Çemen I (2018). Lithospheric structure and the isostatic state of Eastern Anatolia: Insight from gravity data modeling. Lithosphere, 10 (2): 279–290. https://doi.org/10.1130/L685.1

Mckenzie D, Elliott JR, Altunel E, Walker RT, Kurban YC et al. (2016). Seismotectonics and rupture process of the Mw 7.1 2011 Van reverse-faulting earthquake, eastern Turkey, and implications for hazard in regions of distributed shortening. Geophysical Journal International, 206 (1): 501-524. https://doi.org/10.1093/gji/ggw158

Oruç B, Sönmez T (2017). The rheological structure of the lithosphere in the Eastern Marmara region, Turkey. Journal of Asian Earth Sciences, 139: 183-191.

Oruç B, Gomez Ortiz D, Petit C (2017). Lithospheric flexural strength and effective elastic thicknesses of the Eastern Anatolia (Turkey) and surrounding region. Journal of Asian Earth Sciences, 150, 1-13. https://doi.org/10.1016/j.jseaes.2017.09.015

Özacar AA, Gilbert H, Zandt G (2008). Upper mantle discontinuity structure beneath East Anatolian Plateau (Turkey) from receiver functions. Earth and Planetary Science Letters, 269 (3-4): 427-435. https://doi.org/10.1016/j.epsl.2008.02.036

Özalp S, Zabcı C, Elmacı H, Sançar T (2011). 23 Ekim 2011 Van ve 09 Kasım 2011 Edremit (Van) Depremleri. TÜBİTAK Bilim ve Teknik, Aralık, 529: 16-20 (in Turkish).

Özalp S, Aydemir BS, Olgun Ş, Şimşek B, Elmacı H et al. (2015). Van Gölü Doğu Yarısının Kuvaterner Tektoniği ve 23 Ekim 2011 Van Depremi'nin (Mw: 7,2) Kaynak Fay Özellikleri. Maden Tetkik ve Arama Genel Müdürlüğü, Rapor No: 11845: 108 Ankara (in Turkish).

Özalp S, Aydemir BS, Olgun Ş, Şimşek B, Elmacı H et al. (2016). Tectonic deformations in the quaternary deposits of the Lake Van (Edremit Bay), Eastern Anatolia, Turkey. Bulletin of Mineral Research and Exploration 153. https://doi.org/10.19076/mta.65720

Özkaymak Ç, Sözbilir H, Bozkurt E, Dirik K, Topal T et al. (2011). 23 Ekim 2011 Tabanlı-Van Depreminin Sismik Jeomorfolojisi ve Doğu Anadolu'daki Aktif Tektonik Yapılarla Olan İlişkisi. Jeoloji Mühendisliği Dergisi, 35 (2): 175-200 (in Turkish).

Pasyanos ME, Masters TG, Laske G, Ma Z (2014). LITHO1. 0: An updated crust and lithospheric model of the Earth. Journal of Geophysical Research: Solid Earth, 119 (3): 2153-2173. https://doi.org/10.1002/2013JB010626

Pınar A, Honkura Y, Kuge K, Matsushima M, Sezgin N et al. (2007). Source mechanism of the 2000 November 15 Lake Van earthquake (Mw= 5.6) in Eastern Turkey and its seismotectonic implications. Geophysical Journal International, 170 (2): 749-763. https://doi.org/10.1111/j.1365-246X.2007.03445.x

Reilinger R, McClusky S, Vernant P, Lawrence S, Ergintav S et al. (2006). GPS constraints on continental deformation in the Africa-Arabia-Eurasia continental collision zone and implications for the dynamics of plate interactions. Journal of Geophysical Research: Solid Earth, 111 (B5). https://doi.org/10.1029/2005JB004051

Salah MK, Şahin Ş, Aydın U (2011). Seismic velocity and Poisson's ratio tomography of the crust beneath East Anatolia. Journal of Asian Earth Sciences, 40 (3): 746-761. https://doi.org/10.1016/j.jseaes.2010.10.021

Sandvol E, Turkelli N, Zor E, Gok R, Bekler T et al. (2003). Shear wave splitting in a young continent–continent collision: An example from Eastern Turkey. Geophysical Research Letters 30 (24): 8041. https://doi.org/10.1029/2003GL017390

Selçuk AS, Erturac MK, Sunal G, Çakır Z (2020). Evaluation of the Plio-Quaternary tectonic stress regime from fault kinematic analysis in the lake Van Basin (Eastern Anatolia). Journal of Structural Geology, 140: 104157. https://doi.org/10.1016/j.jsg.2020.104157

Singh AP, Mishra OP, Kumar D, Kumar S, Yadav RBS (2012). Spatial variation of the aftershock activity across the Kachchh Rift Basin and its seismotectonic implications. Journal of Earth System Science, 121 (2): 439-451. https://doi.org/10.1007/s12040-012-0175-9

Schildgen TF, Yıldırım C, Cosentino D, Strecker MR (2014). Linking slab break-off, Hellenic trench retreat, and uplift of the Central and Eastern Anatolian plateaus. Earth-Science Reviews, 128: 147-168. https://doi.org/10.1016/j.earscirev.2013.11.006

Stockhecke M, Kwiecien O, Vigliotti L, Anselmetti FS, Beer J et al. (2014). Chronostratigraphy of the 600,000-year-old continental record of Lake Van (Turkey). Quaternary Science Reviews, 104: 8-17. https://doi.org/10.1016/j.quascirev.2014.04.008

Şaroğlu F, Yılmaz Y (1986). Doğu Anadolu'da neotektonik dönemdeki jeolojik evrim ve havza modelleri. MTA dergisi, 107: 73-94 (in Turkish).

Senel M, Ercan T (2002). Geological map of Turkey, 1.500, 000. Van Sheet: General Directorate of Mineral Research and Exploration, Ankara.

Şengör AMC, Kidd WSF (1979). Post-collisional tectonics of the Turkish-Iranian plateau and a comparison with Tibet. Tectonophysics, 55 (3-4): 361-376. https://doi.org/10.1016/0040-1951(79)90184-7

Şengör AMC, Yilmaz Y (1981). Tethyan evolution of Turkey: a plate tectonic approach. Tectonophysics, 75 (3-4): 181-241. https://doi.org/10.1016/0040-1951(81)90275-4

Şengör AMC, Yılmaz Y (1983). Evolution of Neo-Tethyan in Turkey. Turkish Geological Society Special Publication, 75.

Şengör AMC, Özeren S, Genç T, Zor E (2003). East Anatolian high plateau as a mantle-supported, north-south shortened domain structure. Geophysical Research Letters, 30 (24). https://doi.org/10.1029/2003GL017858

Thurber CH (1992). Hypocenter-velocity structure coupling in local earthquake tomography. Physics of the Earth and Planetary Interiors, 75 (1-3): 55-62. https://doi.org/10.1016/0031-9201(92)90117-E

Tezel T, Shibutani T, Kaypak B (2013). Crustal thickness of Turkey determined by receiver function. Journal of Asian Earth Sciences, 75: 36-45. https://doi.org/10.1016/j.jseaes.2013.06.016

Toker M, Ecevitoğlu GB (2012) Shallow seismicity of the Van earthquake (ML, 7.2, 23 October 2011, Eastern Anatolia): monitoring and analysis of the seismic data. In: Proceedings of the national conference with international participation Geosciences 2012, Bulgarian Geological Society (BGS), Sofia, 13-14 December 2012.

Toker M, Pınar A, Tur H (2017). Source mechanisms and faulting analysis of the aftershocks in the Lake Erçek area (Eastern Anatolia, Turkey) during the 2011 Van event (Mw 7.1): implications for the regional stress field and ongoing deformation processes. Journal of Asian Earth Science 150: 73-86 https://doi.org/10.1016/j.jseaes.2017.09.017

Toker M, Şahin Ş (2019). Crustal Poisson's ratio tomography and velocity modelling across tectono-magmatic lake regions of Eastern Anatolia (Turkey): New geophysical constraints for crustal tectonics. Journal of Geodynamics, 131: 101651. https://doi.org/10.1016/j.jog.2019.101651

Toker M, Pınar A, Hoşkan N (2021), An integrated critical approach to off-fault strike-slip motion triggered by the 2011 Van mainshock (Mw 7.1), Eastern Anatolia (Turkey): New stress field constraints on subcrustal deformation, Journal of Geodynamics 147 (101861): 1-25. https://doi.org/10.1016/j.jog.2021.101861

Toker M, Şahin Ş (2022). Upper- to mid-crustal seismic attenuation structure above the mantle wedge in East Anatolia, Turkey: Imaging crustal scale segmentation and differentiation, Physics of the Earth and Planetary Interiors, https://doi.org/10.1016/j.pepi.2022.106908

Turkelli N, Sandvol E, Zor E, Gok R, Bekler T et al. (2003). Seismogenic zones in Eastern Turkey. Geophysical Research Letters 30 (24): 8039. https://doi.org/10.1029/2003GL01823

Utkucu M, Durmuş H, Yalçın H, Budakoğlu E, Işık E (2013). Coulomb static stress changes before and after the 23 October 2011 Van, eastern Turkey, earthquake MW= 7.1: implications for the earthquake hazard mitigation. Natural Hazards and Earth System Science, 137: 1889–1902. https://doi.org/10.5194/nhess-13-1889-2013

Üner T, Mutlu S (2019). Savatlı-Özalp Ofiyolitinde (Van-Doğu Anadolu) Gözlenen Ultramafik Kayaçlar ve İlişkili Mafik Daykların Petrolojik Özellikleri. Çukurova Üniversitesi Mühendislik-Mimarlık Fakültesi Dergisi, 34 (1): 115-128 (in Turkish). https://doi.org/10.21605/cukurovaummfd.601339

Vanacore EA, Taymaz T, Saygın E (2013). Moho structure of the Anatolian Plate from receiver function analysis. Geophysical Journal International, 193 (1): 329-337. https://doi.org/10.1093/gji/ggs107

Wessel P, Smith WHF, Scharroo R, Luis JF, Wobbe F (2013). GMT 5: a major new release of the Generic Mapping Tools. Eos, Transactions of the American Geophysical Union, 94 (45): 409-410.

Wessel P, Smith WH (1998). New, improved version of Generic Mapping Tools released. Eos, Transactions American Geophysical Union, 79 (47): 579-579. https://doi.org/10.1029/98EO00426

Yılmazer M (2003). Deprem kaynak parametrelerinin On-line Belirlenmesi. İstanbul Üniversitesi, Fen Bilimleri Enstitüsü, Yüksek Lisans Tezi, 47 s., İstanbul, Türkiye (in Turkish).

Zor E, Sandvol E, Gurbuz C, Turkelli N, Seber D et al. (2003). The crustal structure of the Eastern Anatolian plateau (Turkey) from receiver functions. Geophysical Research Letters 30: https://doi.org/10.1029/2003GL018192